Euclid P-channel and N-channel comparison

Post-Irradiation Characterisation

[pchanEuclid_TR_03.01]

Issue: 1

Revision: 1

e2v centre for electronic imaging
Planetary and Space Sciences
The Open University
Walton Hall
Milton Keynes, MK7 6AA
United Kingdom

		Date
Prepared by:	Jason Gow, Neil Murray, Andrew Holland, Simeon Barber	7/12/11
Checked by:	Andrew Holland	7/12/11
Authorised by:	Andrew Holland	7/12/11
Internal code:	pchanEuclid_TR_03.01	

The Open University

Document Change Record

Issue/ Revision	Date	Modified pages	Comments
0/1	12/10/11	all	initial draft issue
0/2	8/11/11	all	Corrections incorporated from J. Endicott
1/0	23/11/11	1-2	Initial issue
1/1	7/12/11	all	Minor corrections, included figures on comparing control regions with cosmetics and dark current

Distribution List

Internal	External		
J. Gow	e2v J. Endicott	S. Darby	P. Turner
N. Murray	P. Pool		
A. Holland			
S. Barber			
D. Hall			

Table of Contents

1 Scope

This document describes the post irradiation characterisation of three p-channel CCD204 devices irradiated at KVI, based on the p-channel test plan [1]. Results from measurements of the CTI, dark current and cosmetic quality are discussed as a function of temperature, and compared to results collected as part of the parallel Euclid radiation damage study on the n-channel CCD204 [2-3].

2 Documents

These references are cited at appropriate places in the text and details of the publications are listed here:

1. J. Gow, N. Murray, A. Holland and S. Barber, "*Test Plan: Proton radiation damage assessment of the p-channel CCD204*", pchanEuclid_TP_01.04, 6th December 2010

2. J. Gow, N. Murray, D. Hall and A. Holland, "WP1: CTI Measurements Test Report", Open_Euclid_TR.16.01, 23rd April 2010

3. J. Gow, N. Murray, A. Holland, "Euclid CCD204: Radiation Damage Assessment", Open_Euclid_TR.07.01, 17th August 2011

4. J. Gow, N. Murray, A. Holland, "Comparison of the Radiation Damage Effects in P-channel and N-channel CCDs", p-chan_TP_03.04, 16th October 2009

5. Bebek, C., Groom, S., Holland, S., et. al., "Proton Radiation Damage in P-channel CCDs Fabricated on High-Resistivity Silicon", IEEE Trans. Nucl. Sci., vol. 49, no. 3, pp. 1221-1225, 2002

6. Dawson, K., Bebek, C., Emes, J., et. al., "Radiation Tolerance of Fully-Depleted P-Channel CCDs Designed for the SNAP Satellite", IEEE Trans. Nucl. Sci., vol. 55, no. 3, pp. 1725-1735, 2008

7. N. J. Mostek et al., "Charge trap identification for proton-irradiated p+ channel CCDs", Proc. SPIE, vol. 7742, 2010.

8. J. R. Janesick, "Scientific Charge Coupled Devices", The Society of Photo-Optical Instrumentation Engineers, SPIE Press, Washington, 2001

9. J. P. D. Gow and Neil J. Murray, "Pre-irradiation Characterisation of the p-channel CCD204", Open_pchanEuclid_TN_02.01, 7th July 2010

3   Introduction

The work presented in this report was carried out by the e2v centre for electronic imaging at the Open University as part of an investigation into the post proton irradiation performance of the p-channel CCD204-22. Six p-channel CCD204 devices were available for testing, three of which were selected for proton irradiation.

The key aim of this study was to assess the possible advantages of using a p-channel CCD over an n-channel device, and to investigate any improvements made at e2v on p-channel CCD development compared to the p-channel CCD47 [4].

In 2009 the cei performed the analysis of a p-channel epitaxial CCD47, comparing its performance to that of an n-channel CCD02, full details on this work can be found in [4]. The un-irradiated dark current at 20 °C was found to be twice the typical value for e2v n-channel CCDs, but the increase in dark current with proton fluence was comparable. A comparison of p-channel and n-channel performance at -90 $^{\circ}$C is given in Figure 3.1. Although the p-channel device was indeed more radiation hard the base performance needed to be improved to be comparable with n-channel performance. Bulk (float zone) devices had demonstrated base CTI equivalent to n-channel devices [5-6]; based on this the possible improvement in performance is highlighted in Figure 3.2.
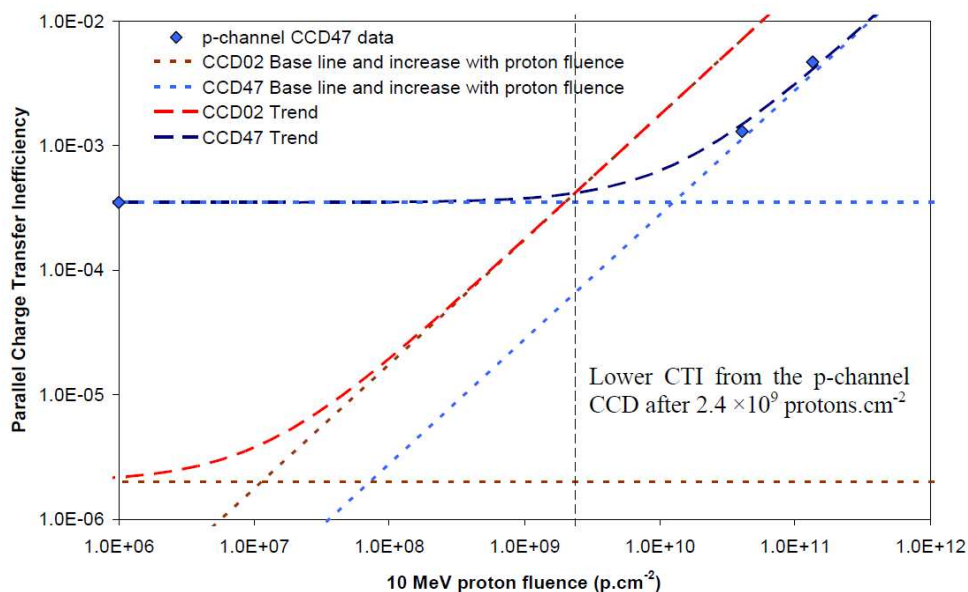
Figure 3.1: Comparison of the p-channel CCD47 parallel CTI with an n-channel CCD02 at -90 °C as a function of proton fluence [4]
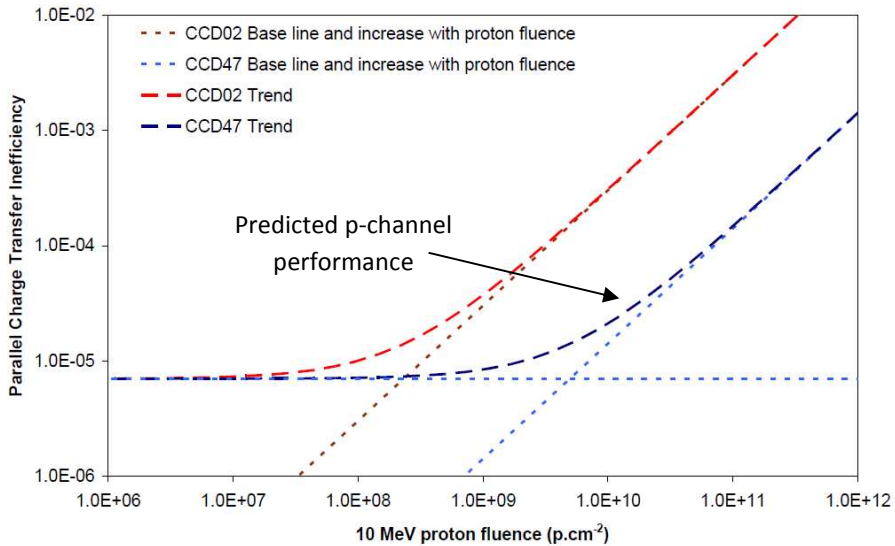
Figure 3.2: Comparison of the p-channel CCD47 parallel CTI with an n-channel CCD02 at -90 °C as a function of proton fluence, assuming the base CCD47 performance was the same as the CCD02 [4]

The p-channel CCD204 device was produced with the aim to improve on the baseline performance and to provide performance similar to that indicated in Figure 3.2. This report summarises the comparison between data collected using n-channel CCD204s, performed as part of the initial Euclid radiation damage assessment, and three p-channel CCD204s fabricated at e2v technologies.

4   Experimental Arrangement

The same physical experimental setup was used as previously employed for n-channel testing, details can be found in [1], with the p-channel CCDs mounted in the same camera system using the same headboard. To allow the same headboard to be used an inverter was created, illustrated in Figure 4.1, to invert the clocks and video output and provide negative bias.
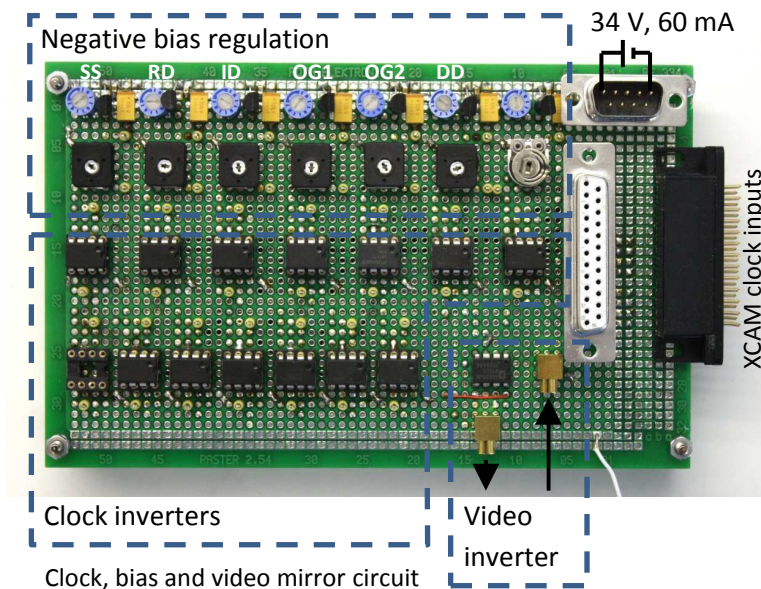
Figure 4.1: Clock, bias and video mirror circuit developed to allow the use of the same drive electronics and CCD headboard used during n-channel data collection

4.1   Correlated Double Sampling Card Selection

A change to the original test plan as agreed with e2v, due to initial time constraints pre-irradiation, led to the initial pre-irradiation investigation into device functionally and cosmetic performance being performed at room temperature using a single channel 16-bit dual slope integration (DSI) correlated double sampling (CDS) card.

When the pre-irradiation characterisation began at cryogenic temperatures using the dual channel 14-bit clamp and sample (CS) CDS card (used for n-channel data collection) an issue with high noise was identified, therefore testing proceeded using the 16-bit single channel CDS card reading out through output node E. The operating potentials used for the data collection are given in Tables 1 and 2 for the biases and clocks respectively. The read noise was measured to be between 7 and 8 h⁻ r.m.s. for each device.

Biases		
	16-bit CDS card	14-bit CDS card
Substrate (VSS)	-0.1 V	-0.1 V
Injection drain (VID)	-24.0 V	-24.0 V
Output drain (VOD)	-27.5 V	-29.0 V
Reset drain (VRD)	-17.0 V	-17.6 V
Dump drain (VDD)	-27.0 V	-27.0 V
Output gate 1 (VOG1)	-3.0 V	-3.0 V
Output gate 2 (VOG2)	-4.0 V	-5.5 V

Table 1: Biases used during pre-irradiation characterisation

Clocks		
	16-bit CDS card	14-bit CDS card
Image	0 to - 8.8 V	0 to - 8.8 V
Serial	0 to - 7.4 V	0 to - 8.8 V
Reset	0 to - 8.0 V	0 to - 8.8 V
Dump gate	0 to -11.0 V	0 to -11.0 V
Injection gate	0 to -11.0 V	0 to -11.0 V

Table 2: Clock potentials used during pre-irradiation characterisation

An issue with the 16-bit DSI CDS card was identified where banding was present within the first ~1500 columns readout, illustrated in Figure 4.2. Pre-irradiation analysis was performed in regions with no banding, i.e. the ADC level across a blank image with no CCD connected is stable to within ±2 ADC channels. The banding was present with no CCD connected and therefore is camera related.

Attempts to identify and rectify the problem with the 16-bit DSI CDS card were not successful; therefore post-irradiation characterisation was performed using the dual channel 14-bit CDS card. The 16-bit DSI card was replaced because accurate CTI measurements could not be made in the un-irradiated control region.
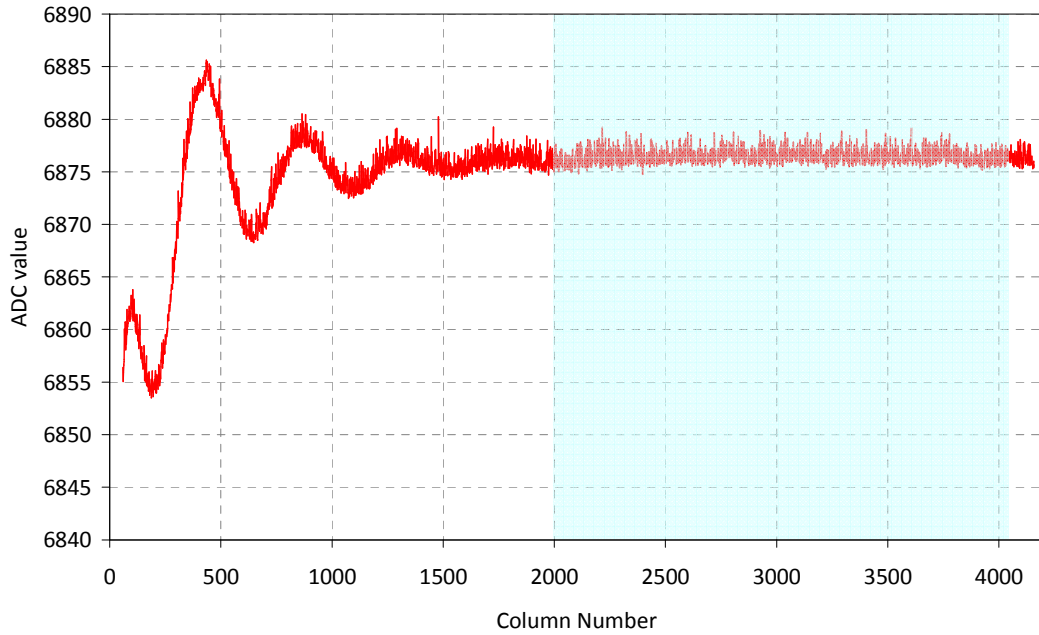
Figure 4.2: Mean ADC level across the column of the CCD showing the banding effect caused by the single channel 16-bit DSI CDS card. The banding is present even when no CCD output is connected.

An investigation into the noise performance and poor spectral performance previously identified when using the using the 14-bit CS CDS card was performed, identifying poor spectral performance for readout through node F. This was resolved by increasing VOG2, as illustrated in Figure 4.3, VRD was also increased to improve the noise performance. The serial clock was increased to be inline with parallel resulting in no change in performance and reset clock was increased to ensure correct operation (at 8.0 V a small amount of serial deferred charge was identified). The operating potentials used for the data collection using the 14-bit CDS are given in Tables 1 and 2 for the biases and clocks respectively. The read noise reduced to 11-12 h$^-$ r.m.s. for each device.
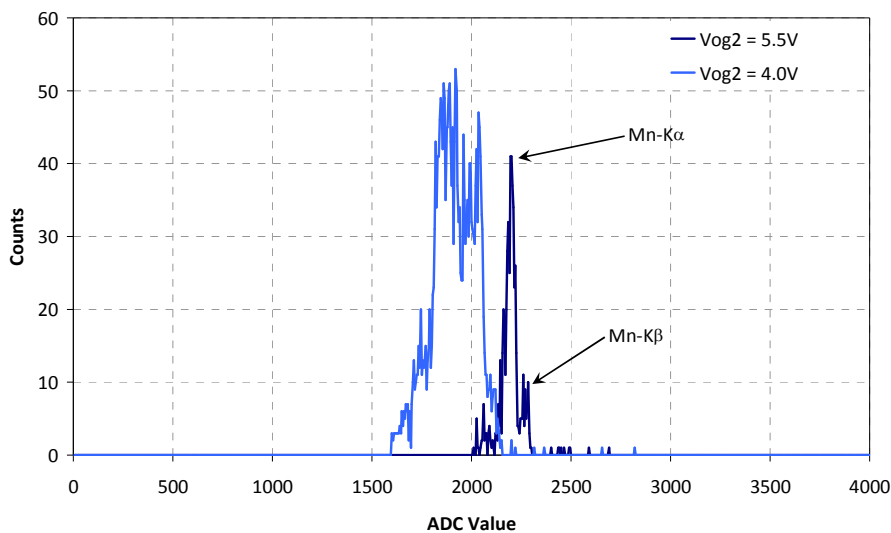
Figure 4.3: Resulting peak from Mn-Kα and Mn-Kβ X-ray events incident on a p-channel CCD at 210 K using different VOG2 potentials

To ensure that the modifications did not change pre-irradiation performance an un-irradiated p-channel control, 10092-06-02, was examined at 140 K and 170 K. The CTI and dark current performance was found to be comparable to the two 10092 devices pre-irradiation performance and testing proceeded.

5 Experimental Technique

The equipment technique is described in detail in document [1]. The task was to compare the CTI, dark current and cosmetic quality of the p-channel CCD204 with its n-channel counterpart, as a function of proton damage at different temperatures. Both devices were operated under the same conditions; for convenience a summary is given below.

- 200 kHz readout rate
- Integration time of 500 s
- 90 s pause between successive image acquisitions
- X-ray density of 1 event per 80 pixels

5.1 X-ray CTI Measurement Technique

The CTI measurements were performed using the X-ray technique, which for convenience is described below.

Initially a region of interest (ROI) is selected, Figure 5.1, typically a region that contains either un-irradiated or irradiated pixels. The ROI is then divided into bins 40 pixels wide to identify X-ray event locations to be used in the measurement of parallel and serial CTI respectively, as illustrated in the example in Figure 5.1. Analysis code is then used to collect event location information from a number of images, the peak location within each bin is identified by fitting a Gaussian to the X-ray events within that bin, Figure 5.2. The CTI is then measured using the gradient of the line of best fit applied to the data, Figure 5.3, and the X-ray signal $X(e^-)$, in the form [8]

$$CTI_X = \frac{S_D(e^-)}{X(e^-)n_t} \tag{1}$$

where $S_D(e^-)$ is the average deferred charge, and n_t is the number of pixels transfers. The error on the CTI is calculated using the error on the weighted mean of the peak location and the error on the gradient, found using a parallelogram of error. The error from the equipment is taken as $\pm$ 2 ADC channels. The measurement of CTI using X-rays is described as an absolute measurement of CTI [8].

In cases where the CTI was poor and the fitting routine did not provide a fit, as in the case of the readings in the irradiated regions at 200 K and for all readings with device 10092-02-02, a manual fit to the data was implemented. The error on manual measurements was taken to be 30% of the measurement.

Cross section used to make serial CTI measurements

Cross section used to make parallel CTI measurements
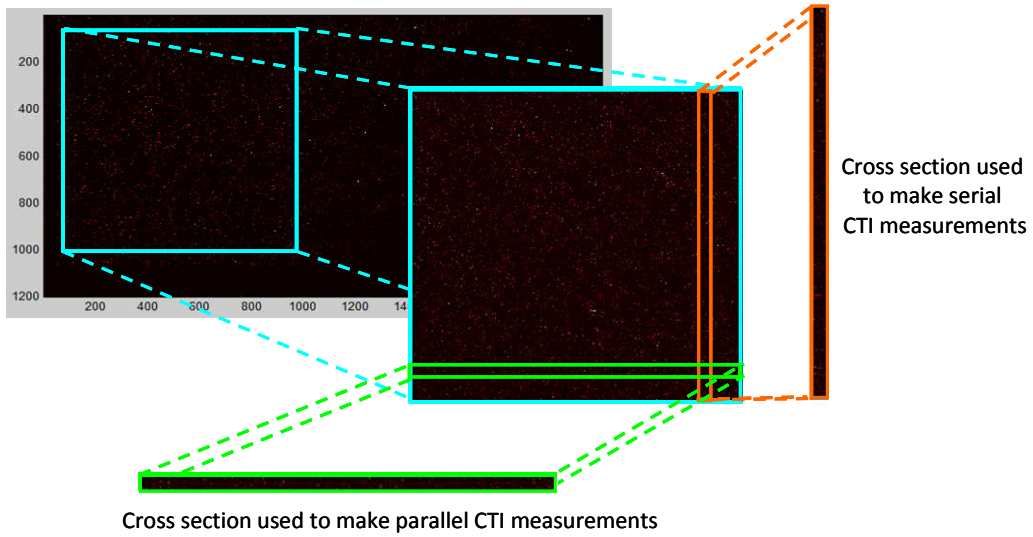
Figure 5.1: Illustration of the selection of a region of interest and bins 40 pixels wide used to measure the parallel and serial CTI
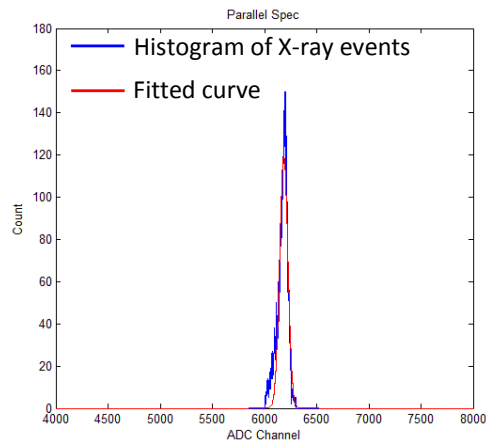
Figure 5.1: Example of the Mn-Ka X-ray peak and the resulting fit used to determine the peak location within one of the bins created across a region of interest
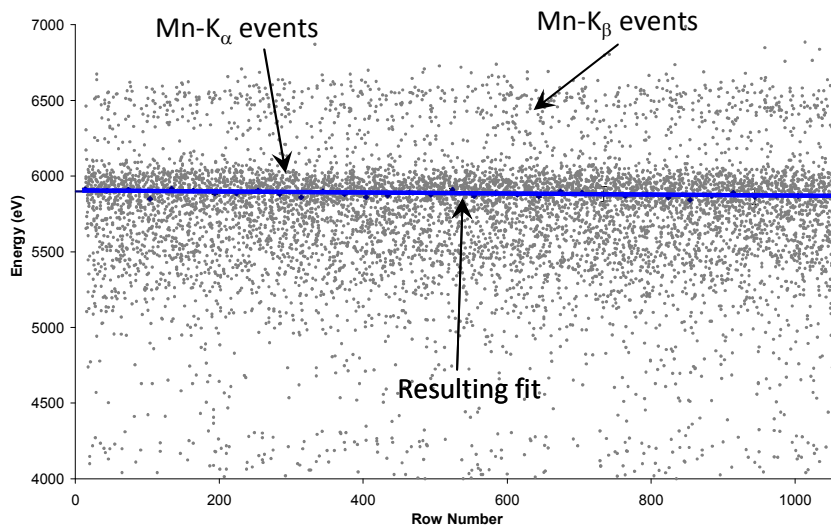
Figure 5.3 X-ray event location and the resulting fit used to measure CTI

6   Pre-irradiation Characterisation

Pre-irradiation performance is covered in detail in document 9; a summary is provided here for convenience.

Devices from batch #10092 were produced from wafers with a single side polished (standard), while devices from batch #10152 were produced from double side polished wafers (these are not normally used for CCD production, but were available from another programme). The latter demonstrated a significantly lower cosmetic quality, as illustrated in Figures 6.1 and 6.2 which show an image taken with devices from batch #10152 and #10092 at room temperature respectively. The horizontal lines at the edge of the images are charge injection and the vertical lines are smeared out point defects.
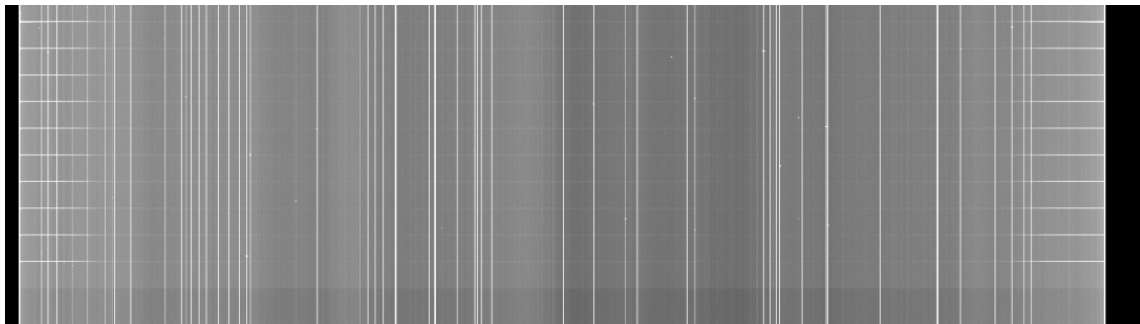
Figure 6.1: Dark image at room temperature taken with device #10152-01-03, with 1/10th second frame integration and ~23 second readout
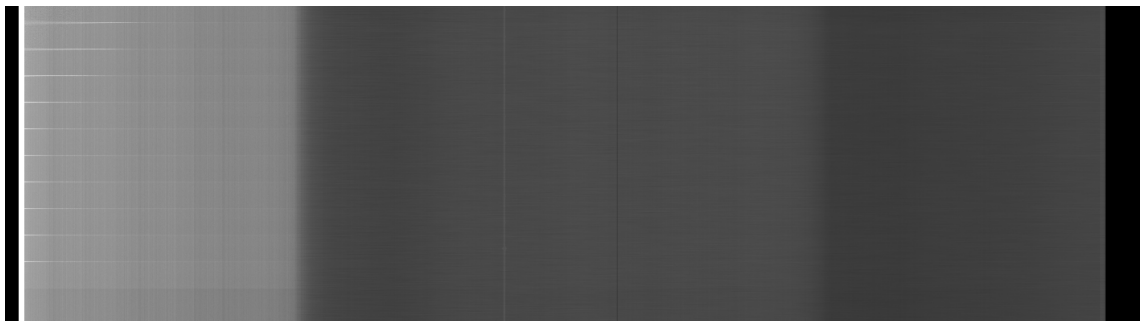
Figure 6.2: Dark image at room temperature taken with device #10092-02-02, with 1/10th second frame integration and ~23 second readout

Comparing the effects of the image electrode load capacitances between the p-channel and n-channel devices yielded similar results, as illustrated in Figure 6.3. For reasons currently unknown the capacitive loading appears to be far lower than in previous p-channel devices manufactured by e2v (CCD227-10, CCD228-80 and CCD47-20); an example of the CCD47 image clock potentials is given in Figure 6.4.
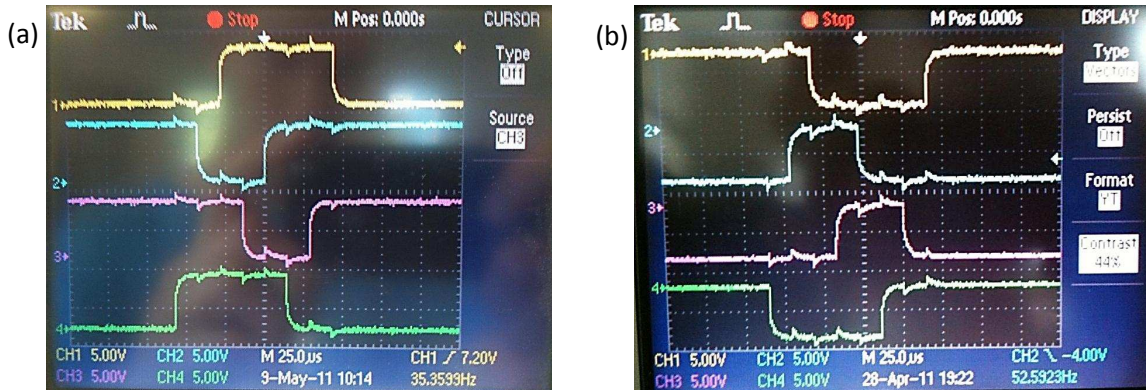
Figure 6.3: Comparison of the image clock potentials between the n-channel CCD204-22 (#05316-07-02) (a) and the p-channel CCD204-22 (#10152-01-03) (b)
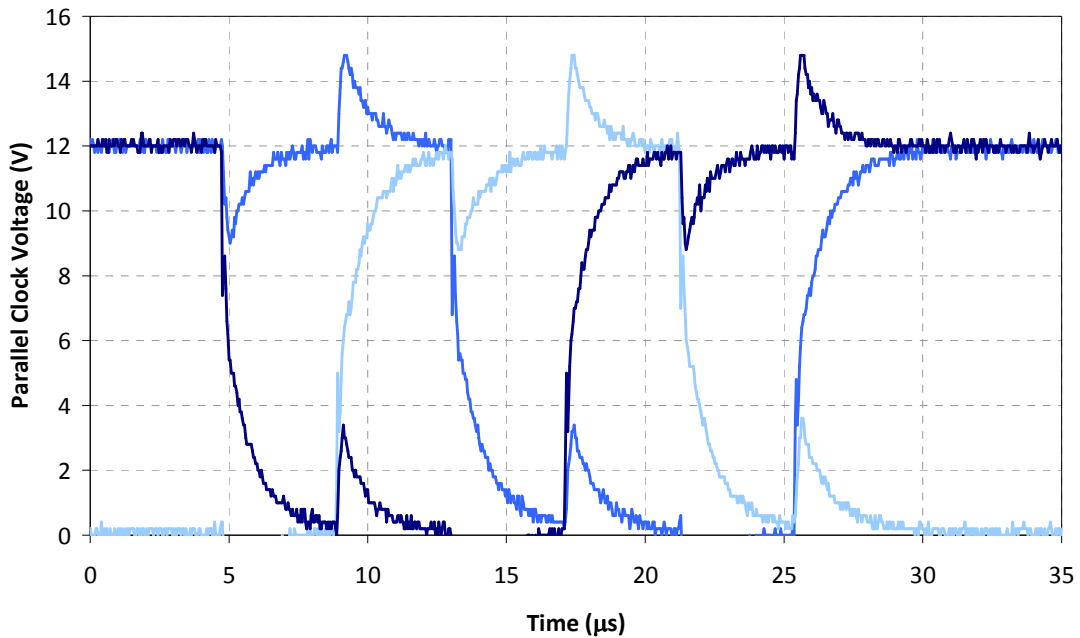
Figure 6.4: Image clock potentials of a p-channel CCD47 [4]

6.1 Cosmetic quality

The percentage of bright pixels presented as a function of temperature is illustrated in Figure 6.5. A bright defect is defined as any pixel exhibiting an ADC value greater than 5σ after an integration time of 500 s, where σ is the standard deviation of the noise peak. The two devices from batch #10092 follow a similar trend to an n-channel CCD204, where data was collected from an un-irradiated region. The bright defects in device #10152-01-03 are as a result of a large number of bright columns, Figure 6.1. Even at -93 °C, there were eight bright columns originating from eight different defects. The large number of bright columns is believed to be the reason why the device does not follow the same trends as the n-channel or other p-channel CCDs, as illustrated in Figure 6.5.
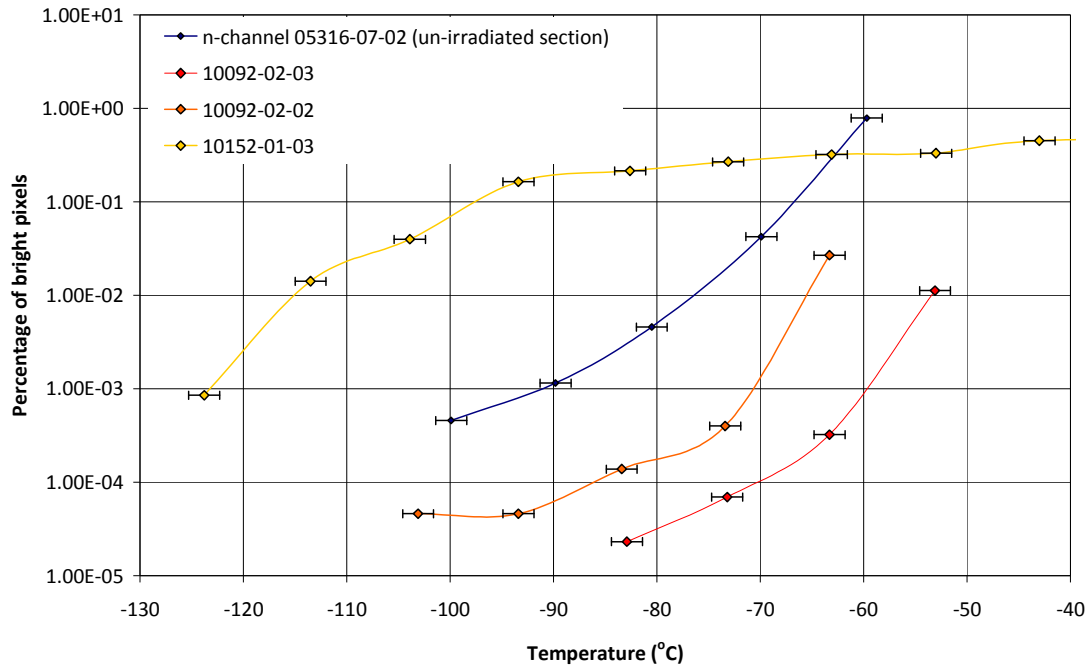
Figure 6.5: Comparison of the percentage of bright pixels as a function of temperature

6.2 Dark current

The dark current was measured as a function of temperature. The results are displayed in Figure 6.6 compared with those of an un-irradiated section of n-channel CCD204 #05316-07-02. The dark current is around twice that of the n-channel CCD204, being around 3 $nA.cm^{-2}$ at room temperature. However, the n-channel CCD204 is front illuminated while the p-channel CCD204 is back illuminated. N-channel back illuminated CCDs have a typical dark current of between 2-3 $nA.cm^{-2}$ at room temperature, therefore the pre-irradiation dark current of the back illuminated p-channel CCD204 appears to be comparable.

Initially the mean background level at low temperatures appeared to be around 20 h^+ after 500 s, however, after examining the analysis code a mistake was identified and corrected (i.e. the ROI selected was incorrect). Read noise was measured to be between 7 and 8 h^- r.m.s. for each device using the 16-bit DSI CDS card and between 11 and 12 h^- r.m.s. for each device using the 14-bit CS CDS card.
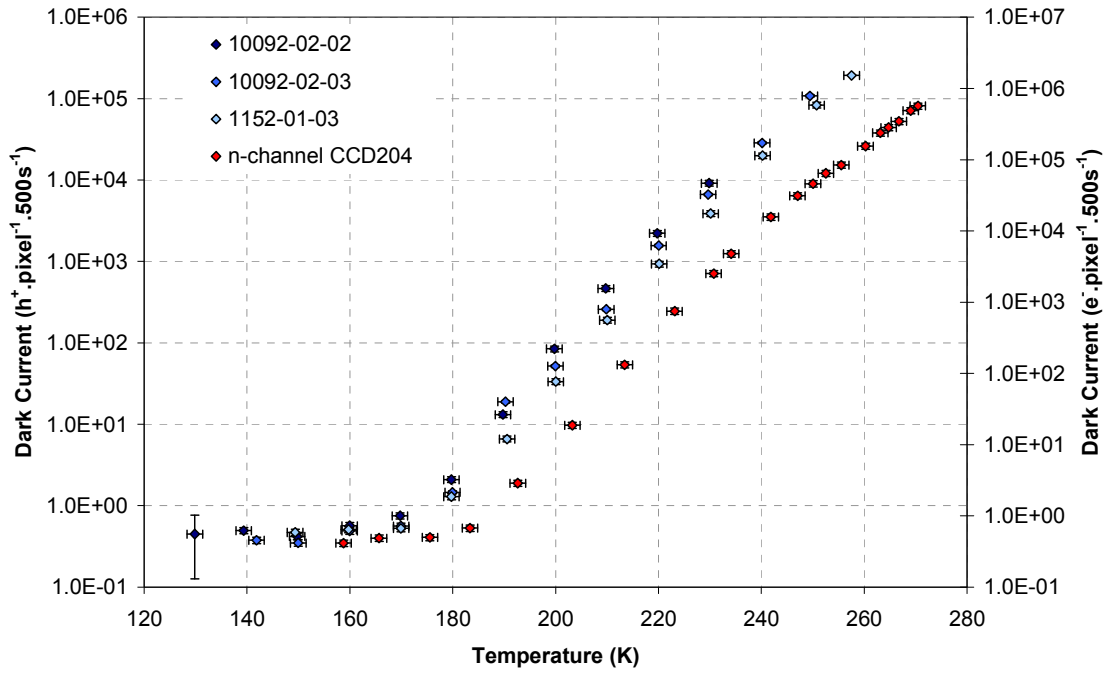
Figure 6.6: Comparisons of the dark current as a function of temperature

6.3   Charge injection

Charge was injected as per the OU method used during the n-channel CCD204 analysis [3], where the input diode is held at a reference level and charge is injected by pulsing the input gate. The data sheet method holds the input gate at a fixed level while pulsing the input diode. When the inverting board was developed the data sheet method was not in use. The injection structure was found to be operational on each device and, as illustrated in Figure 6.7, demonstrated similar uniformity to that of the n-channel CCD204 #05316-07-02 illustrated in Figure 6.8.
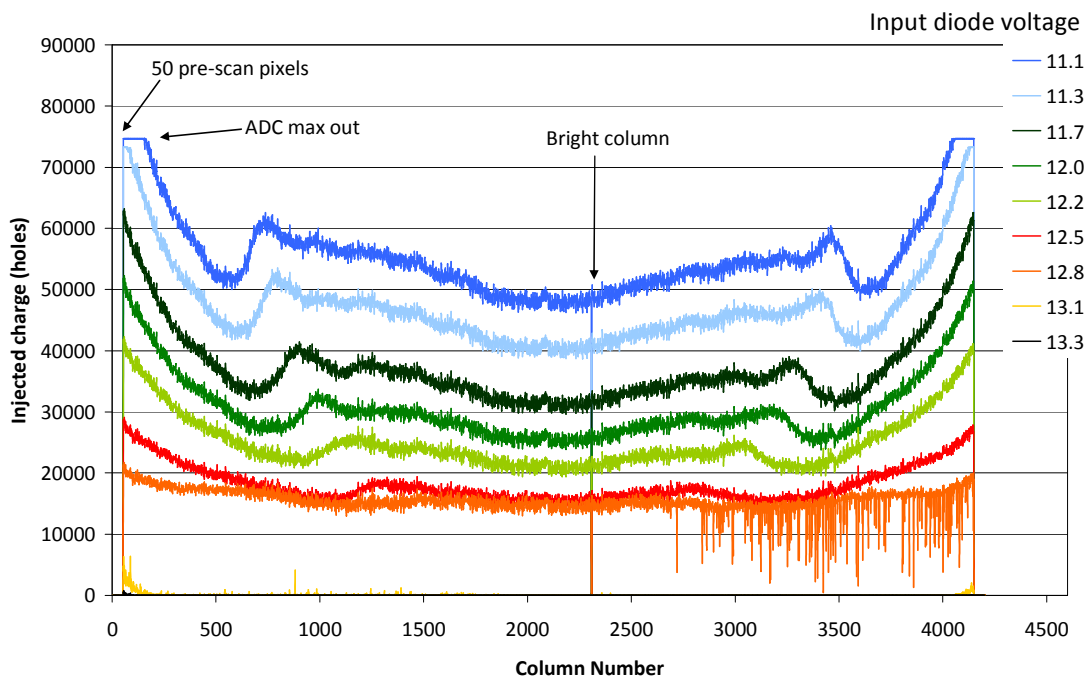
Figure 6.7: Injection uniformity of the p-channel CCD # 10092-02-02 as a function of injection levels
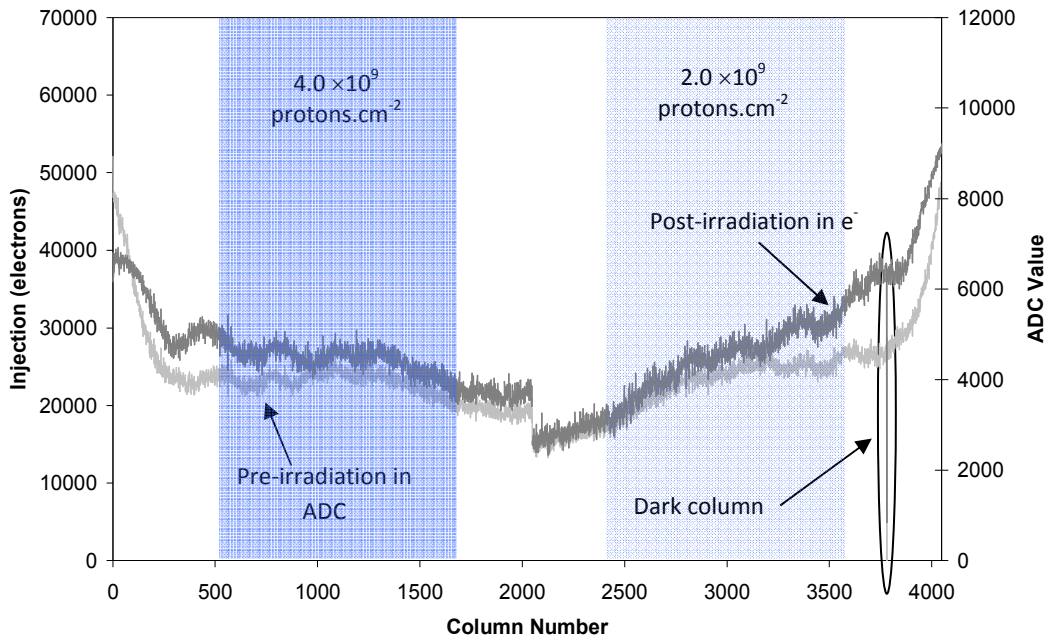
Figure 6.8: Injection uniformity of the n-channel CCD #05316-07-02

6.4 Charge transfer inefficiency

The CTI was measured using Mn-Kα X-ray events. Both the parallel and serial CTI were found to be comparable with n-channel performance, demonstrating a clear improvement in device manufacture (through the use of bulk material) over that used previously. The parallel CTI and serial CTI measured as a function of temperature and compared to the un-irradiated section of the n-channel CCD #05316-07-02 are illustrated in Figure 6.9 and 6.10 respectively, with the inclusion of trend lines to illustrate the apparent trend in CTI. Device #10092-02-03 was re-tested after the bond wire protectors were modified by e2v to ensure it was still operational, results were within error.
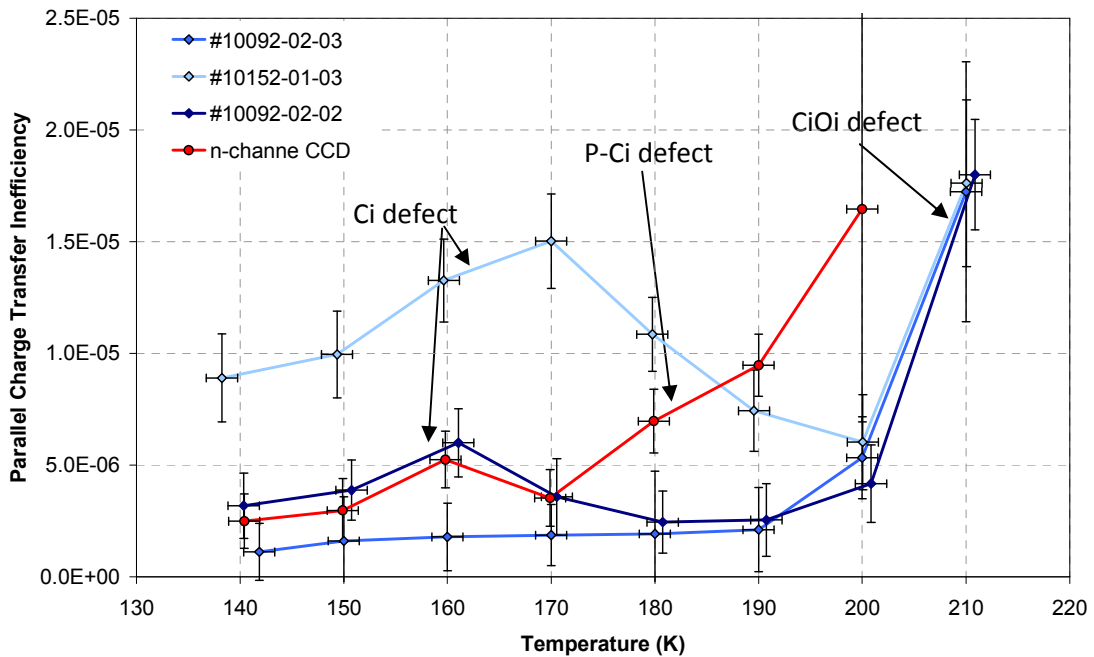
Figure 6.9: Comparison of parallel CTI as a function of temperature, the traps that could be responsible for the trends are also illustrated
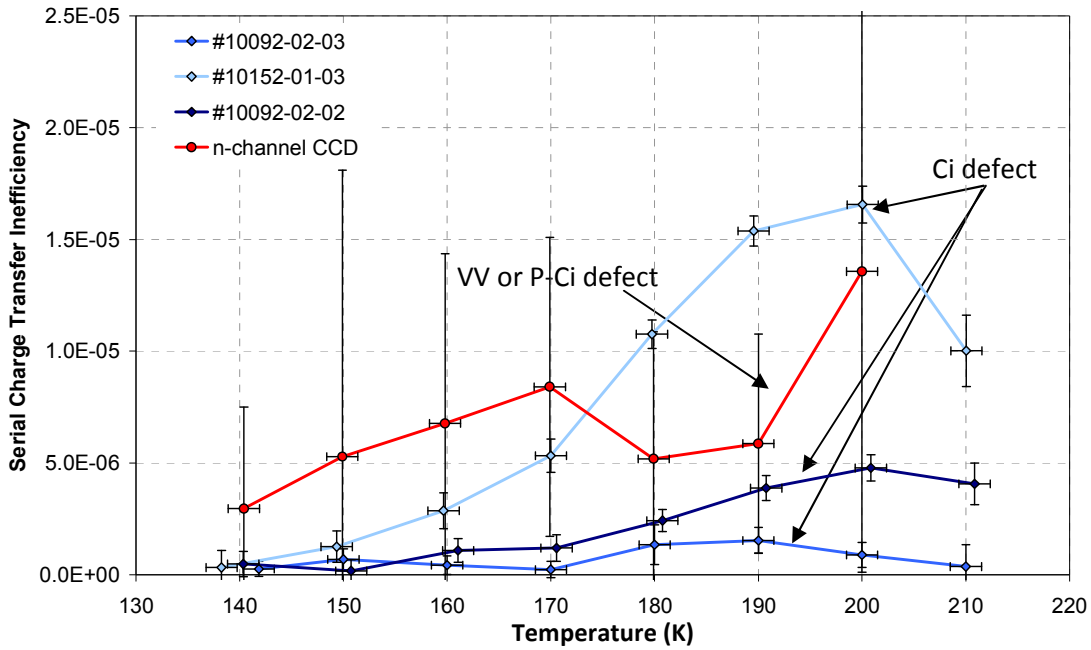
Figure 6.10: Comparison of serial CTI as a function of temperature, the traps that could be responsible for the trends are also illustrated

Operation between 140 K and 165 K, nominal Euclid operating temperature, appears ideal. Both figures clearly indicate an increase in the number of traps present within device #10152-01-03 as a result of having both sides of the silicon wafer polished, resulting in increased CTI. The labels indicating which trap is responsible for the observed trends in CTI are based on the emission times of hole defects reported by Mostek *et al* 2010 [7].

7   Proton Irradiation

The devices were irradiated with 50 MeV protons, produced using the Accelerateur Groningen-ORsay (AGOR) cyclotron at the Kernfysisch Versneller Instituut (KVI) in Holland on the 21st of June 2011. The irradiation levels delivered to the devices are given in Table 3, the area of irradiation is illustrated in Figure 7.1. The devices were collected on the 12th of July and the post irradiation analysis began on the 8th of August 2011.

Device No.	Image area	50 MeV proton fluence (protons.cm^{-2})	50 MeV flux (protons.cm^{-2}.s^{-1})	10 MeV equivalent proton fluence (protons.cm^{-2})
10092-02-03	AE	4.0×10^{9}	2.0×10^{7}	2.0×10^{9}
	AF	8.0×10^{9}	2.0×10^{7}	4.0×10^{9}
10152-01-03	AE	1.6×10^{10}	2.0×10^{7}	8.0×10^{9}
	AF	2.0×10^{10}	2.0×10^{7}	1.0×10^{10}
10092-02-02	AE	1.0×10^{11}	2.0×10^{7}	5.0×10^{10}
	AF	2.0×10^{11}	2.0×10^{7}	1.0×10^{11}

Table 3: Device numbers and irradiation levels delivered at KVI
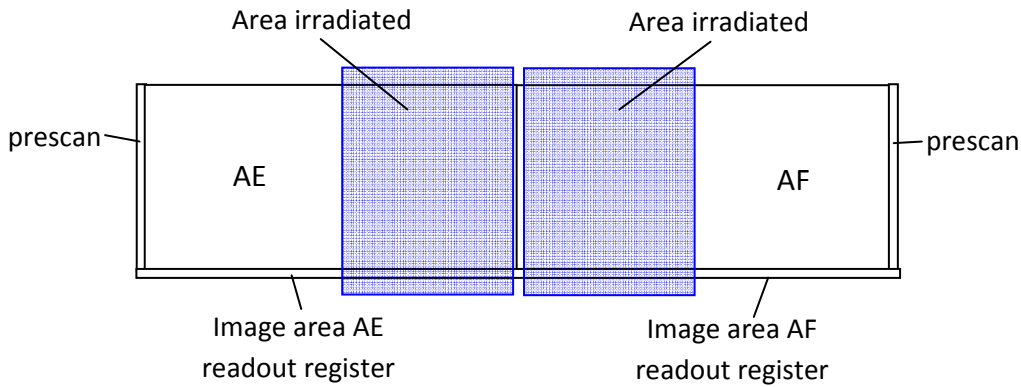
Figure 7.1: Diagram of the CCD204-22, highlighting the areas that were irradiated

8   Post Irradiation Characterisation

Device #10092-02-03 was confirmed as operational at room temperature and then cooled to 140 K at which point data collection for CTI analysis proceeded. During CTI analysis it became apparent that the CTI levels within the control regions had changed for both parallel and serial CTI, the change is illustrated in Figure 8.1 and Figure 8.2. Initially device #10092-02-03 was run through until 180 K and the effect was evident at each temperature. The device was then replaced with device #10152-01-03 and a similar change in the control region was evident. The correct operation of the camera was confirmed by re-mounting the control device, #10092-06-02, measuring the CTI at 170 K. Device #10092-02-02 was then mounted and also exhibited the same effect, as illustrated in Figures 8.1 and 8.2. Testing then proceeded as per the test plan.
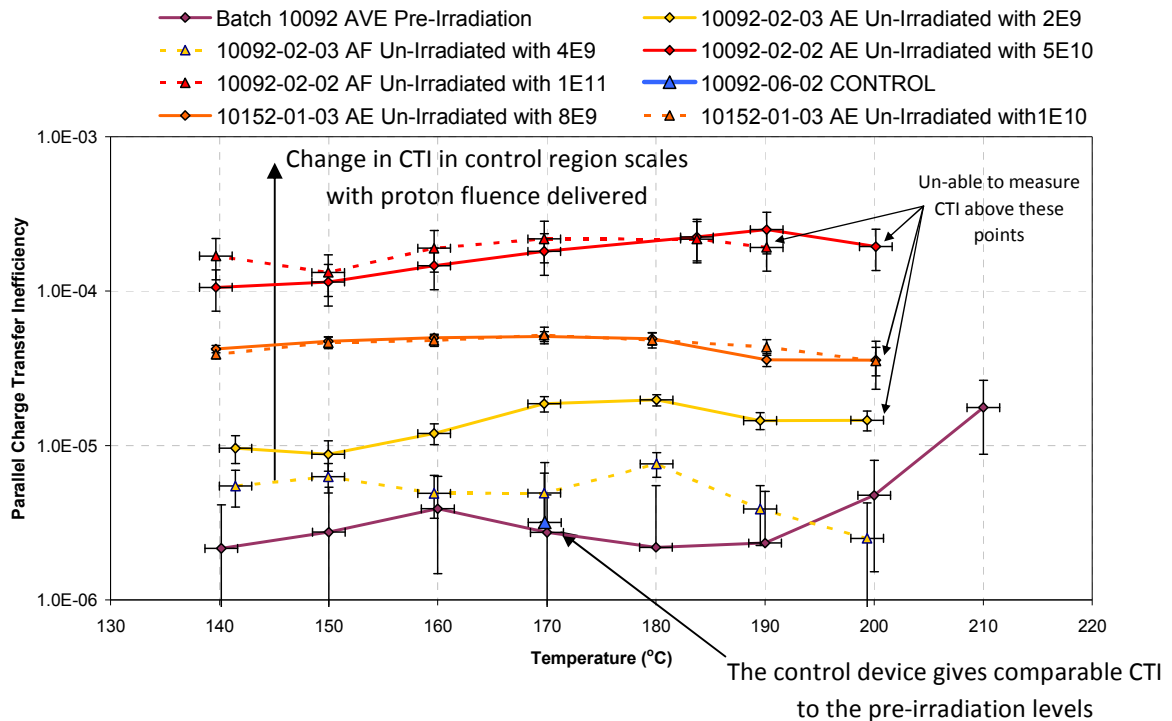
Figure 8.1: Parallel CTI as a function of temperature measured in the un-irradiated control regions and compared with the pre-irradiation average and the un-irradiated device 10092-06-02
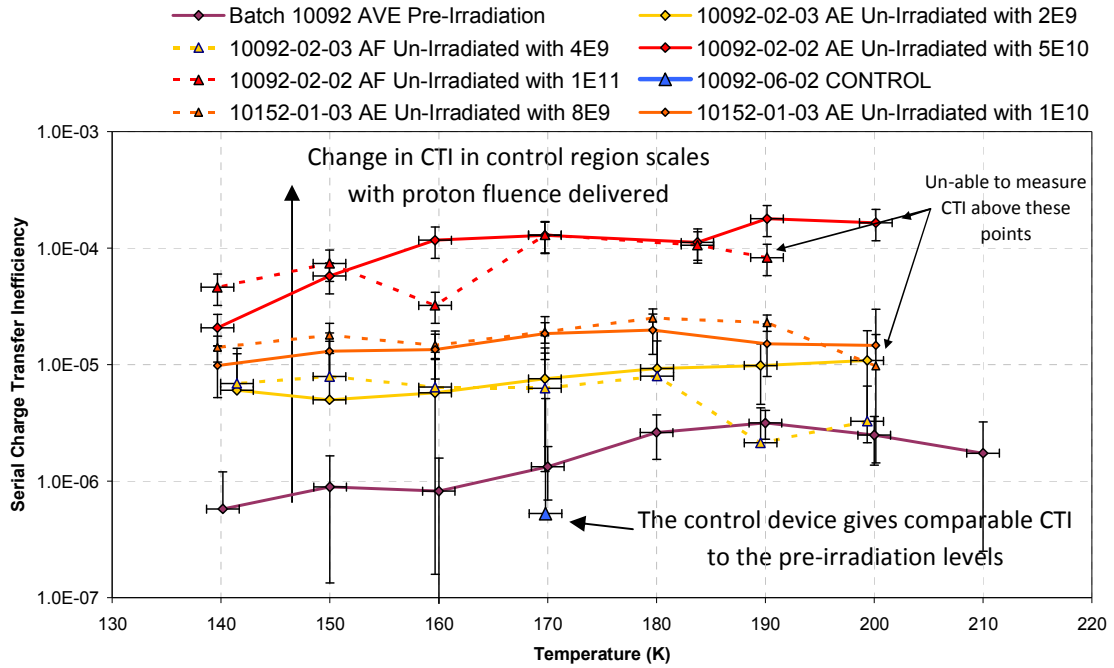
Figure 8.2: Serial CTI as a function of temperature measured in the un-irradiated control regions and compared with the pre-irradiation average and the un-irradiated device 10092-06-02

Comparing the dark current measured in the control regions, Figure 8.3, of the other two CCDs irradiated to a higher level indicates an increase in dark current. However, the increase in dark current is within the experimental error on device 10152-01-03 and almost within error on device 10092-02-02. The error arises from the temperature measurement to ± 1.5 K and the error on the dark current measurement, which relates to peak fitting and the calibration. Analysis of the bright defects generated within the control regions provides clear evidence of radiation damage, i.e. the number of bright defects in the control region of device #10092-02-02 pre-irradiation was measured to be 0 at 190 K while post irradiation 10394 bright defects were identified.
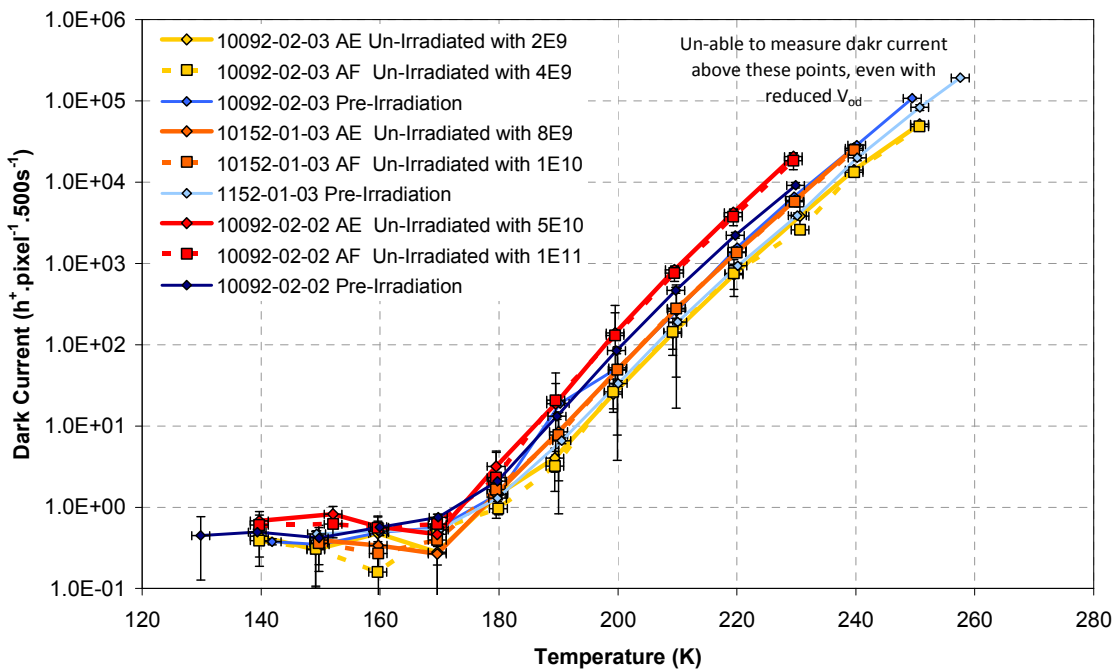
Figure 8.3: Dark current measured pre and post irradiation in the control areas

Three possible explanations are suggested for the cause of radiation damage to the shielded areas, relating to (a) proton damage (b) damage by activation of the CCD package and (c) neutron damage.

With respect to protons, damage might arise if protons were not stopped within the copper shield. However it requires around 4 mm of copper to stop a 50 MeV proton and the shields used were 10 mm thick so this seems unlikely.

With respect to the dose from activation of the CCD package, the dose is very much less than 0.1% of the dose of the irradiation, therefore it is also unlikely that this is the cause.

With respect to neutrons, it is understand from discussions with KVI staff that the neutron flux is approximately 2% of the proton flux. The copper shield would be insufficient to stop neutrons from travelling through the CCD therefore neutron damage is a possible source of the change in control region performance. Neutron interaction would create defect clusters, causing a decrease in the CTI across the CCD and the creation of bright defects but with only a small effect on the overall dark current in the CCD. It is tentatively concluded that the change in the control regions of the CCDs irradiated is most likely to be the result of neutron damage. Note that in future studies the neutron flux could in principle be reduced by using a lower energy primary proton beam.

The increase in CTI illustrated in Figures 8.1 and 8.2 is similar for both sides of the CCD; the increase in dark current in each imaging area is also similar as indicated in Figure 8.3 and in Figure 8.4 for improved clarity. This suggests that the cause is affecting both sides of the CCD to a similar degree. The number of cosmetics created in the control region (for the same area), illustrated in Figure 8.5 at 190 K for CCDs from batch #10092, does not appear to comparable for the CCDs irradiated to the same level. However, in both CCDs irradiated the number of bright defects generated in the control region is lower for the side of the device which received the highest proton fluence.
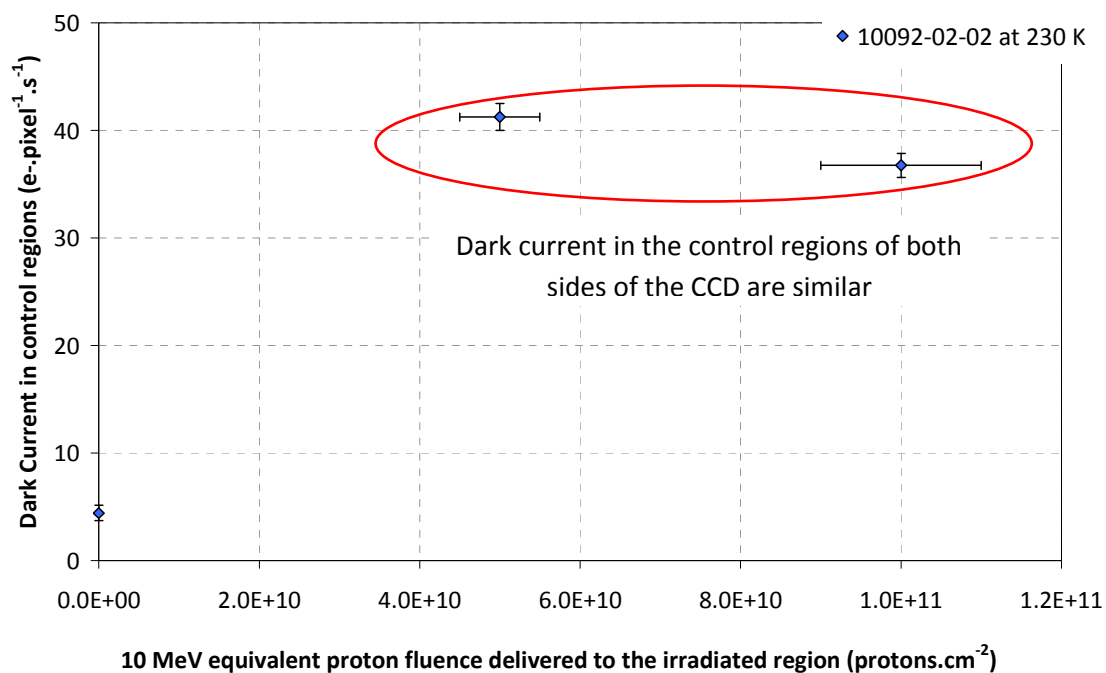
Figure 8.4: Dark current measured in device #10092-02-02 at 230 K in the control region as a function of proton fluence delivered to the irradiated region
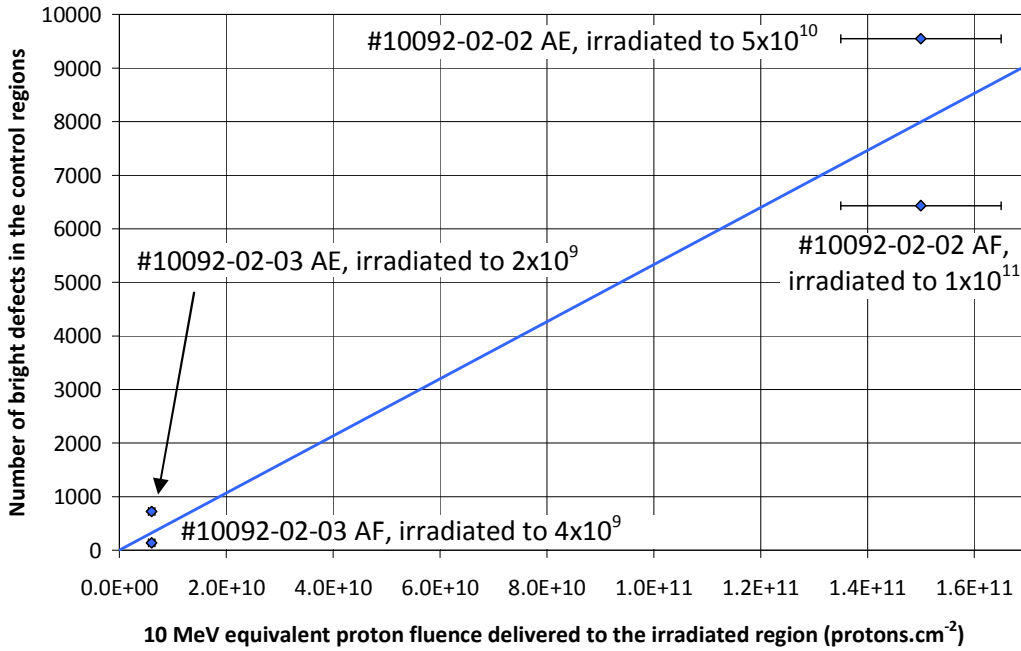
Figure 8.5: Number of bright defects in the two CCDs irradiated from bath #10092 as a function of the total proton fluence delivered to the CCD

It is important to be clear that notwithstanding the above discussion on changes in the performance of the control regions, the vast majority of damage is created by protons. Therefore the testing performed in the current study is valid. See later for recommendations for future work to address the neutron damage hypothesis.

8.1   Cosmetic quality

The numbers of bright defects identified post irradiation and pre-irradiation are illustrated in Figure 8.6. Results from device #10152-01-03 have not been included in the comparison due to the large number of bright defects present in the CCD prior to the irradiation. When compared to the results from the n-channel study, Figure 8.7 [3], the p-channel CCDs clearly demonstrate a greater number of bright defects. The poor CTI in device #10092-02-02 caused bright defects to be smeared, hence the number of bright defects identified with the analysis code is lower than for device #10092-02-03.
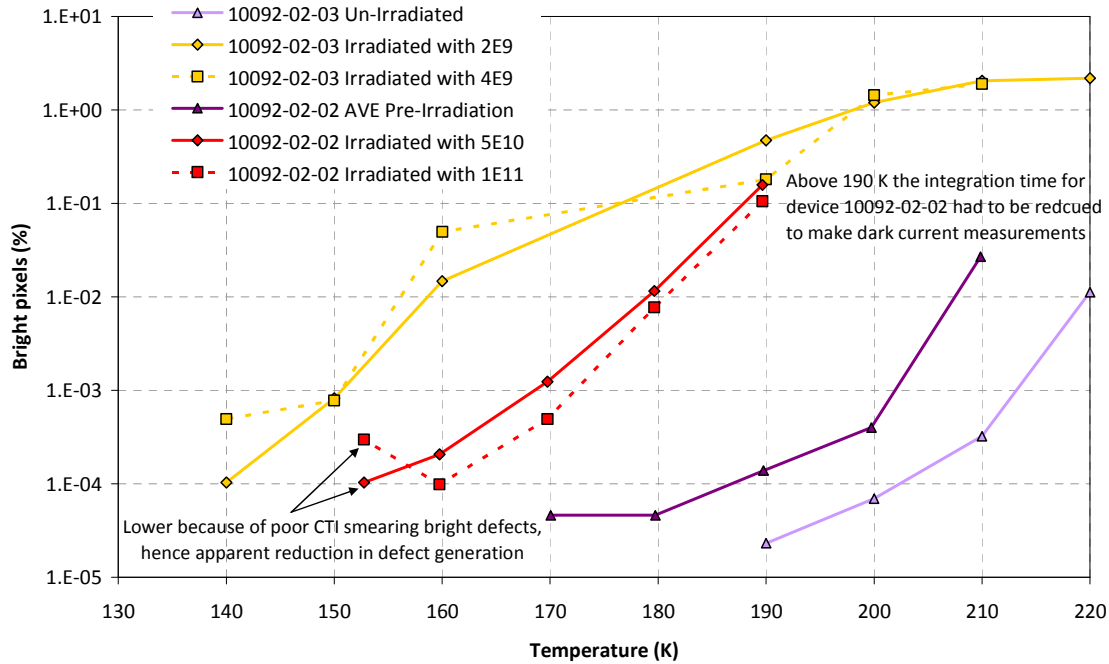
Figure 8.6: Comparison of the percentage of bright pixels pre and post irradiation as a function of temperature
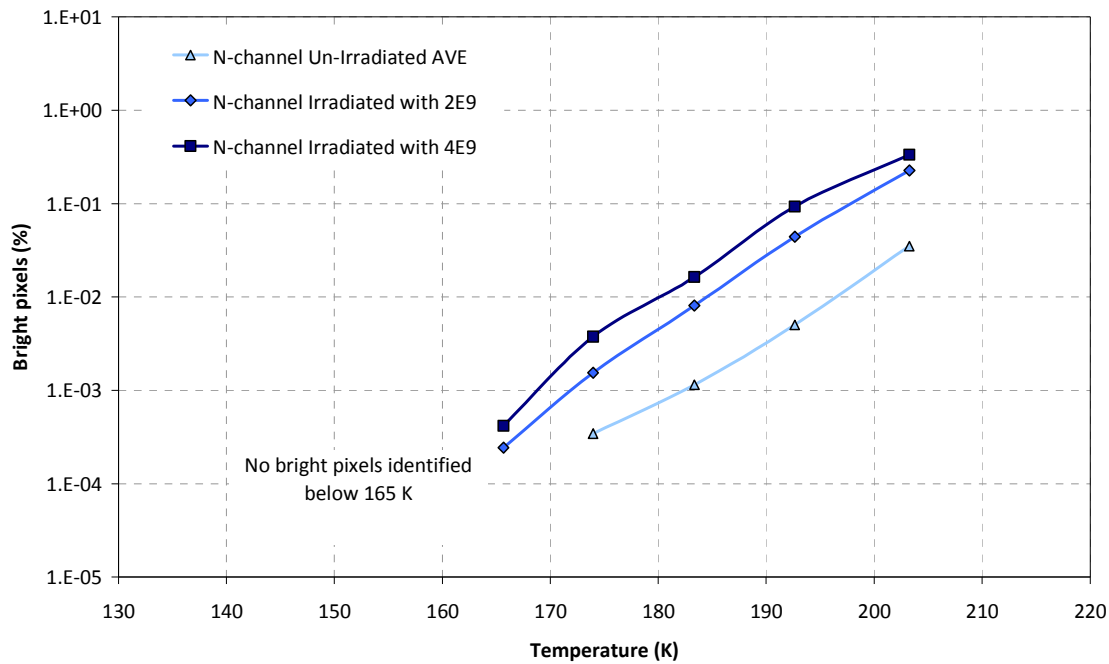
Figure 8.7: Comparisons of the percentage of bright pixels in the n-channel CCD204 devices as a function of temperature

8.2 Dark current

The dark current as a function of temperature, shown in Figure 8.8, was recorded using a 500 seconds integration time between 140 K and 250 K. The measured dark current for both un-irradiated and irradiated sections of the CCD at and below 160 K is comparable. Therefore dark current would not affect performance under Euclid style operating conditions. When comparing the

increase in dark current as a function of proton fluence of the p-channel and n-channel CCDs, illustrated in Figure 8.9, the p-channel CCDs increases by around a factor of 2 more than the n-channel CCD. This could be due to different batches of silicon being used in manufacture, although the definitive reason is currently unknown.
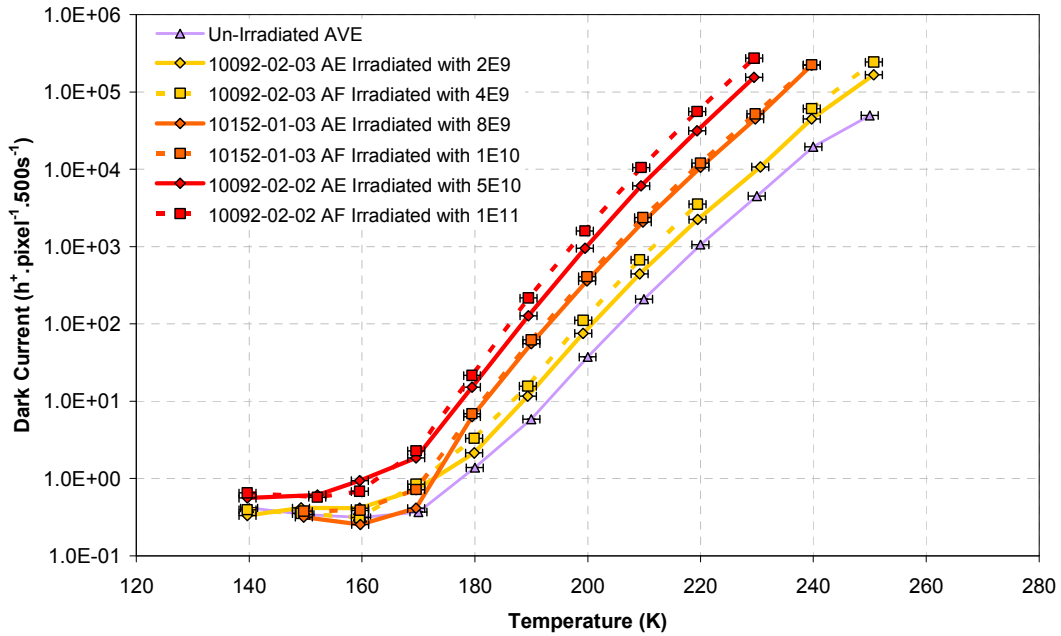
Figure 8.8: Comparison of the p-channel dark current as a function of temperature
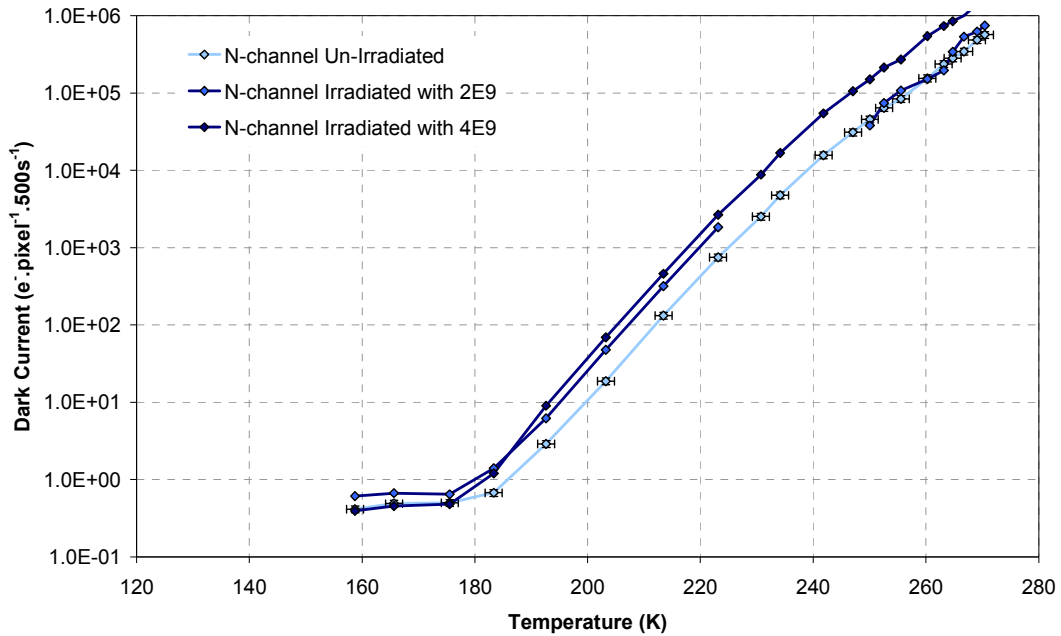
Figure 8.9: Comparison of n-channel dark current as a function of temperature

8.3 Charge injection

The charge injection structure was confirmed to be operational post irradiation in devices 10092-02-03 and device 10152-01-03, as illustrated in Figure 8.10, with no discernable changes from the

pre-irradiation performance. However, device 10092-02-02, Figure 8.11, exhibited a reduction in the amount of injected charge in the irradiated regions of the device as a result of a flatland voltage shift affecting the input gate. If the injection was performed as per the data sheet then this effect would not be observed.
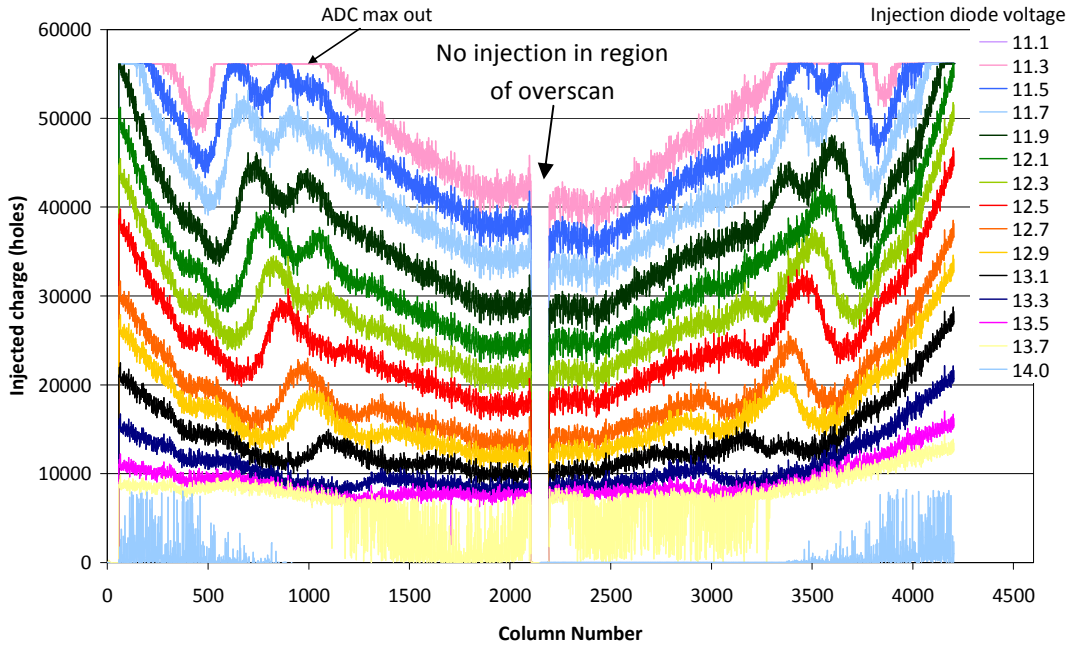
Figure 8.10: Injection uniformity of the p-channel CCD #10152-01-03 as a function of injection levels post irradiation
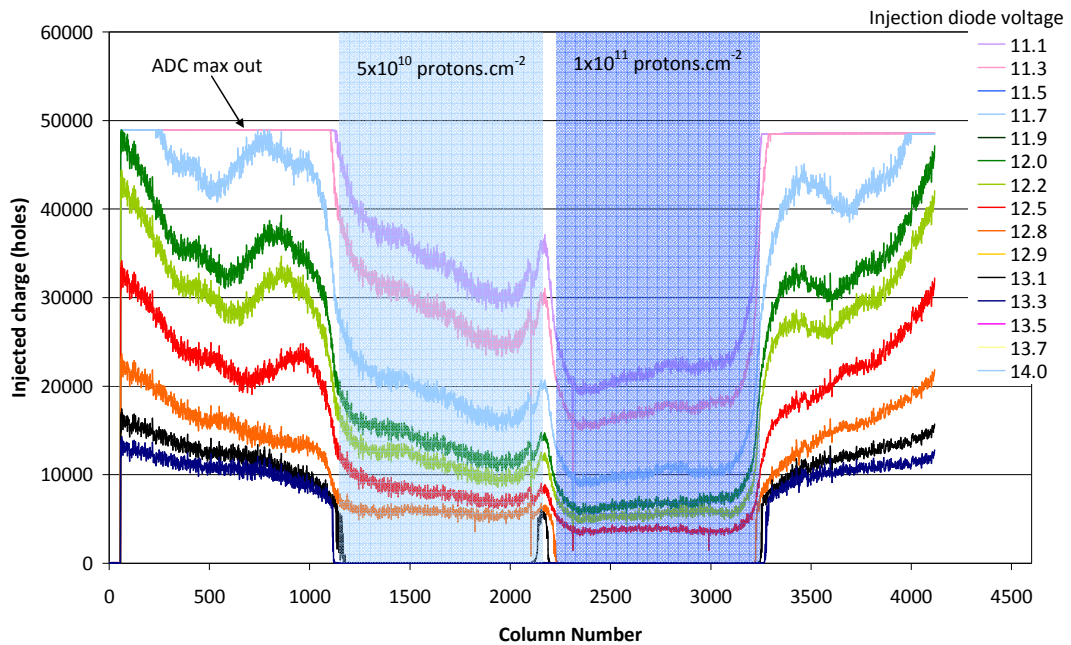
Figure 8.11: Injection uniformity of the p-channel CCD #10092-02-02 as a function of injection levels post irradiation, the overscan between each image has been removed

8.4   Charge transfer inefficiency

The parallel and serial CTI measured using the p-channel CCDs are illustrated in Figures 8.12 and 8.13 respectively, showing the change in CTI as a function of temperature. The parallel and serial CTI of n-channel and p-channel CCDs irradiated to the same proton fluence are compared in Figures 8.14 and 8.15 respectively. The parallel CTI measured using the p-channel CCDs is consistently higher than the CTI measured using the n-channel CCD until the 190 K, where the advantage of p-type silicon and the decreased impact of the electron trapping E-centre becomes evident. The opposite occurs for the serial transfers where the p-channel CCD offers improved performance at 140 K because it is not affected by the electron trapping A-centre defect.
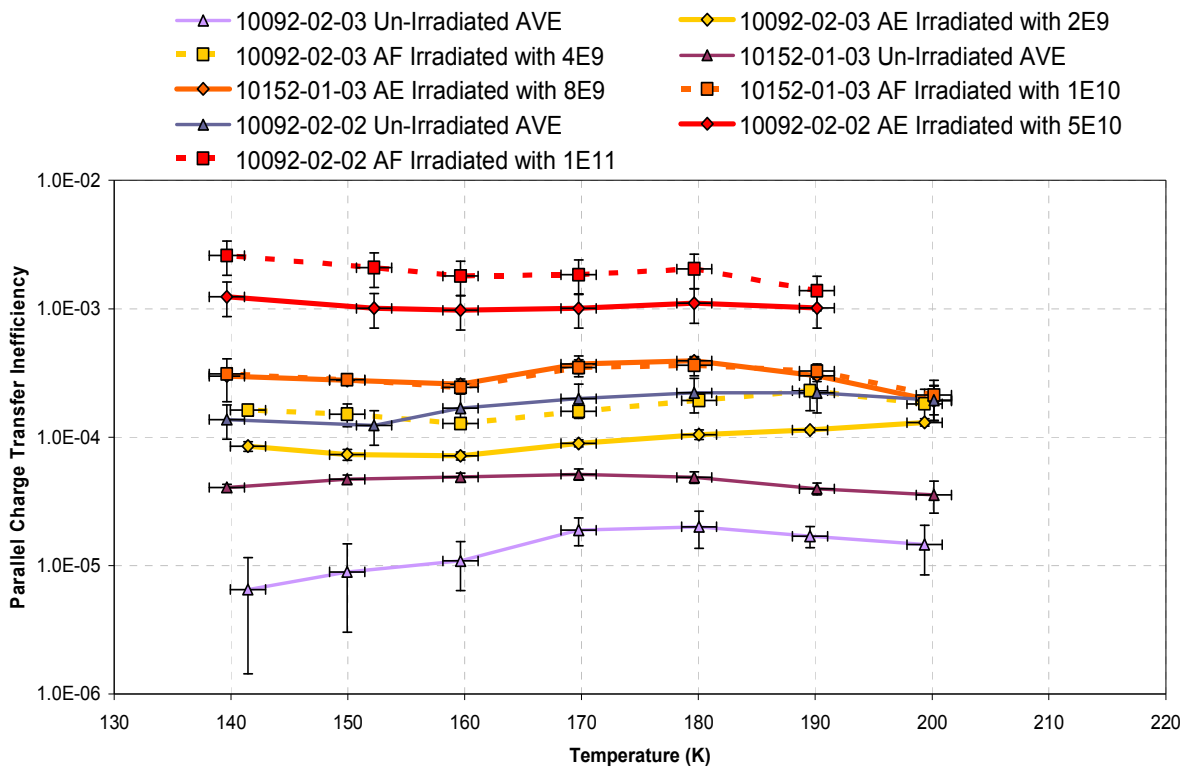
Figure 8.12: Parallel CTI as a function of temperature measured using p-channel CCD204s
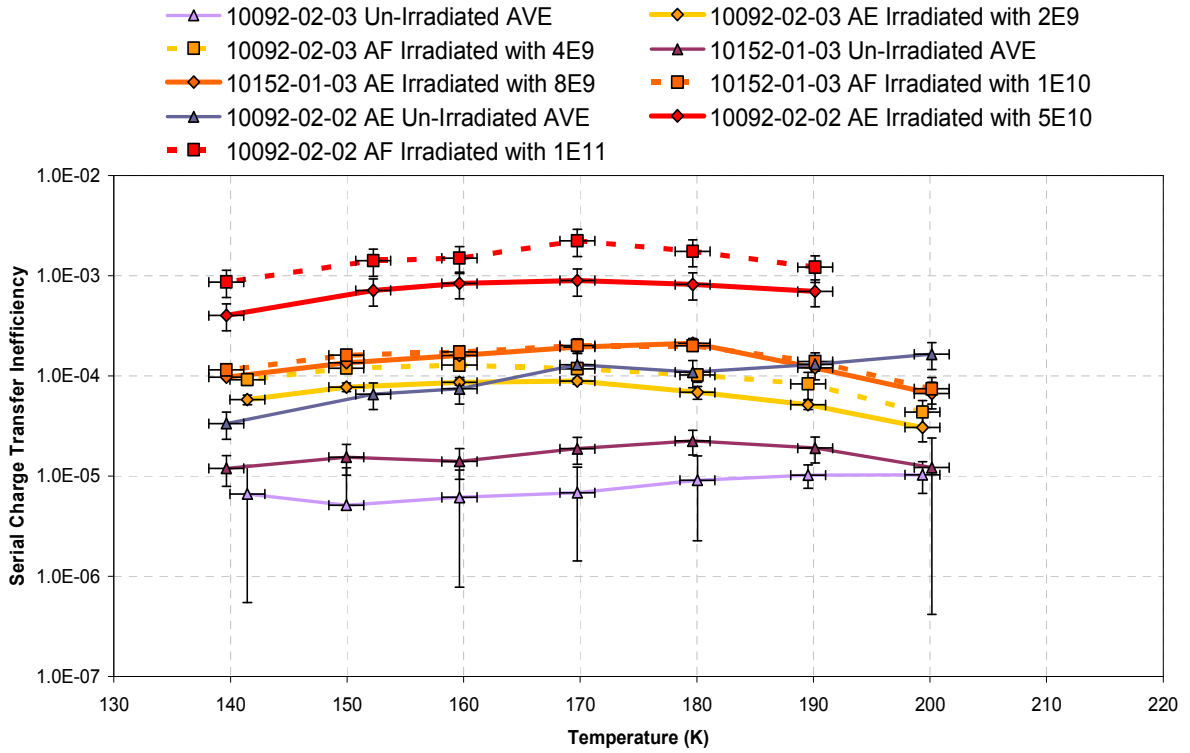
Figure 8.13: Serial CTI as a function of temperature measured using p-channel CCD204s
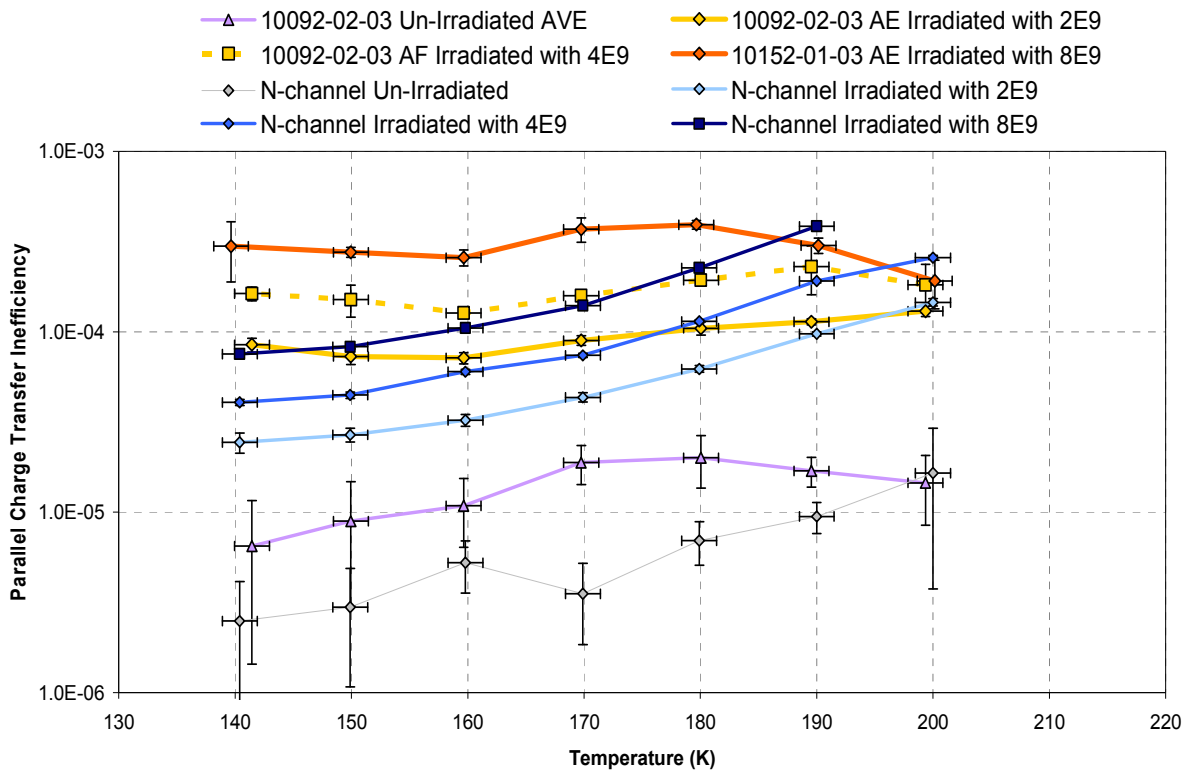
Figure 8.14: Parallel CTI as a function of temperature measured using p-channel
and n-channel CCD204
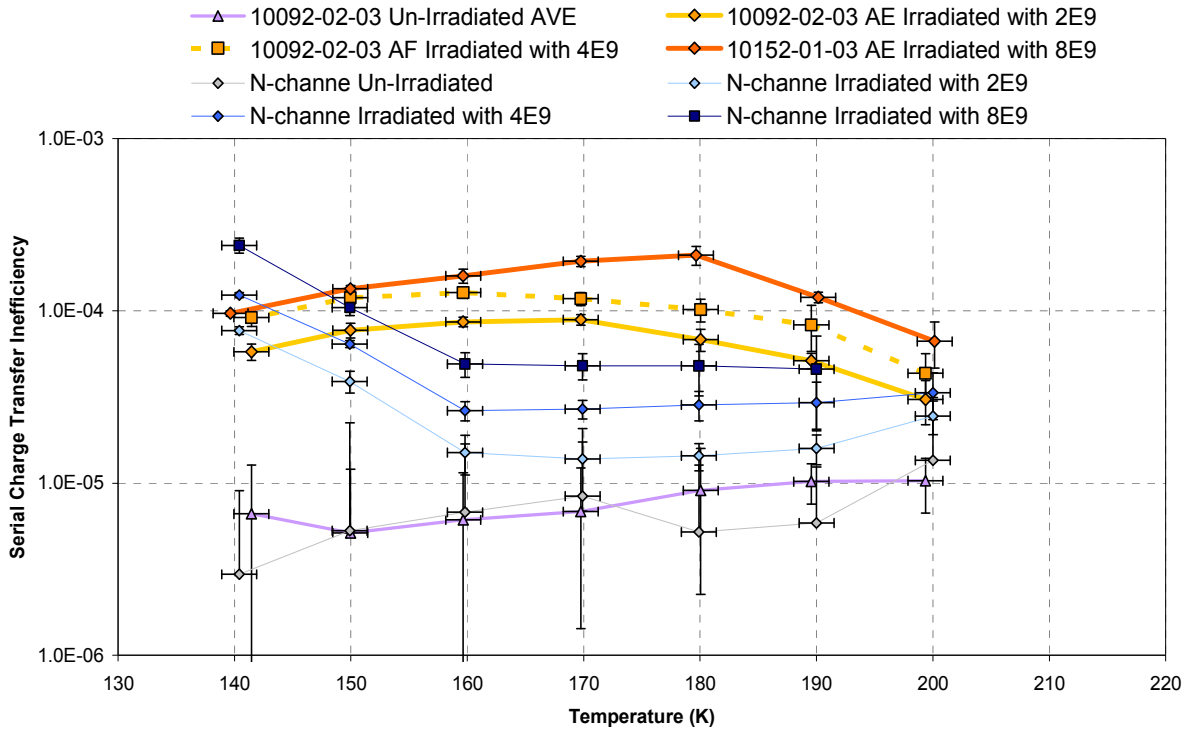
Figure 8.15: Serial CTI as a function of temperature measured using p-channel and n-channel CCD204

9   N-channel and P-channel CTI comparison

The parallel and serial CTI as a function of proton fluence measured across the nominal Euclid operating range is illustrated in Figures 9.1 through to 9.6.
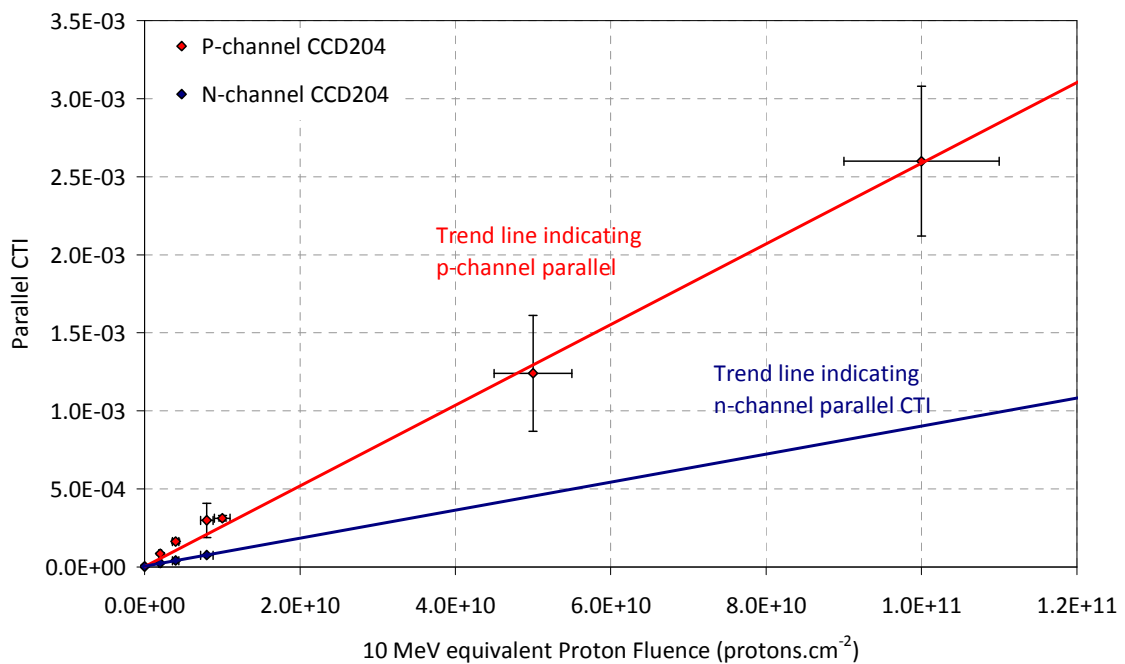
Figure 9.1: Comparison of the parallel CTI measuring using the p-channel with an n-channel CCD204 at 140 K
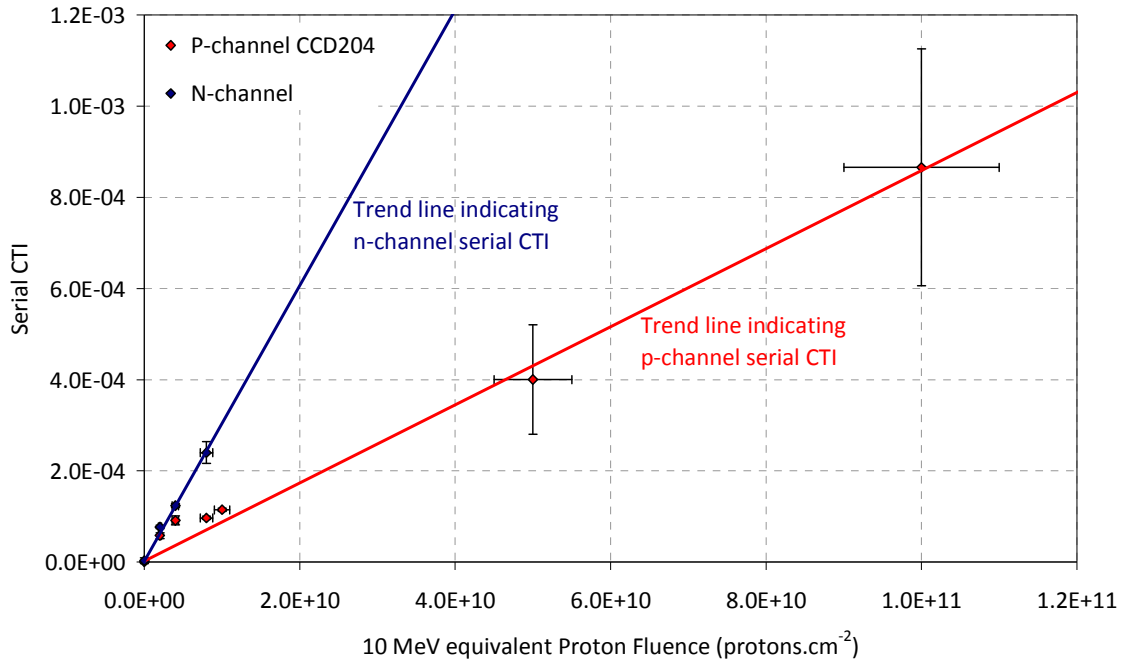
Figure 9.2: Comparison of the serial CTI measuring using the p-channel with an n-channel CCD204 at 140 K
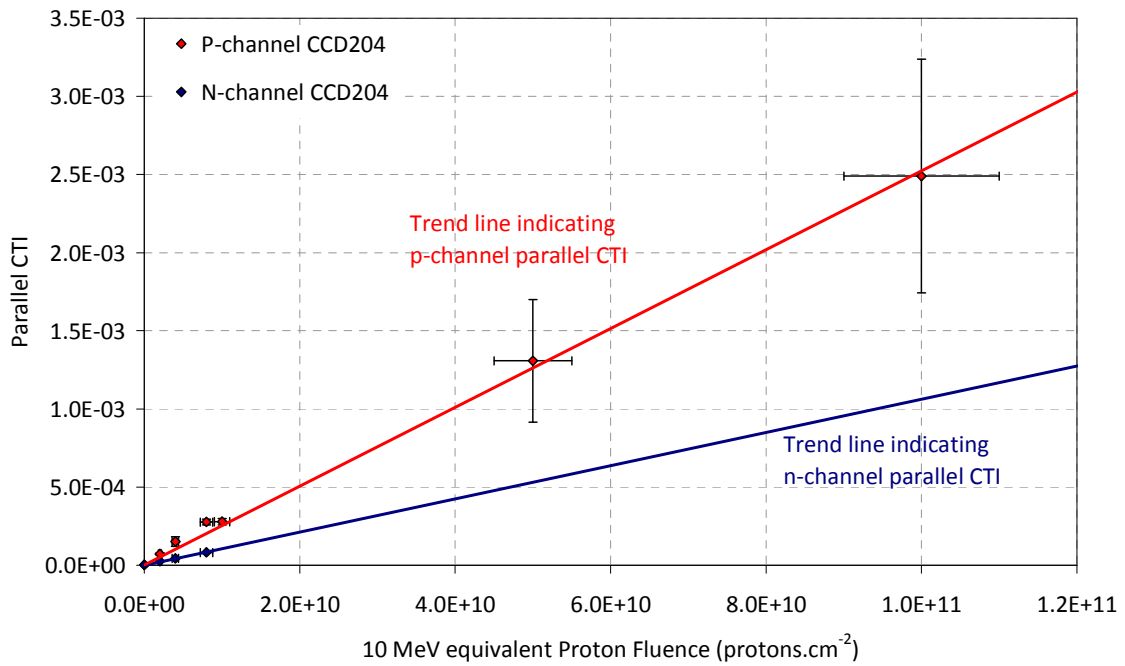
Figure 9.3: Comparison of the parallel CTI measuring using the p-channel with an n-channel CCD204 at 150 K
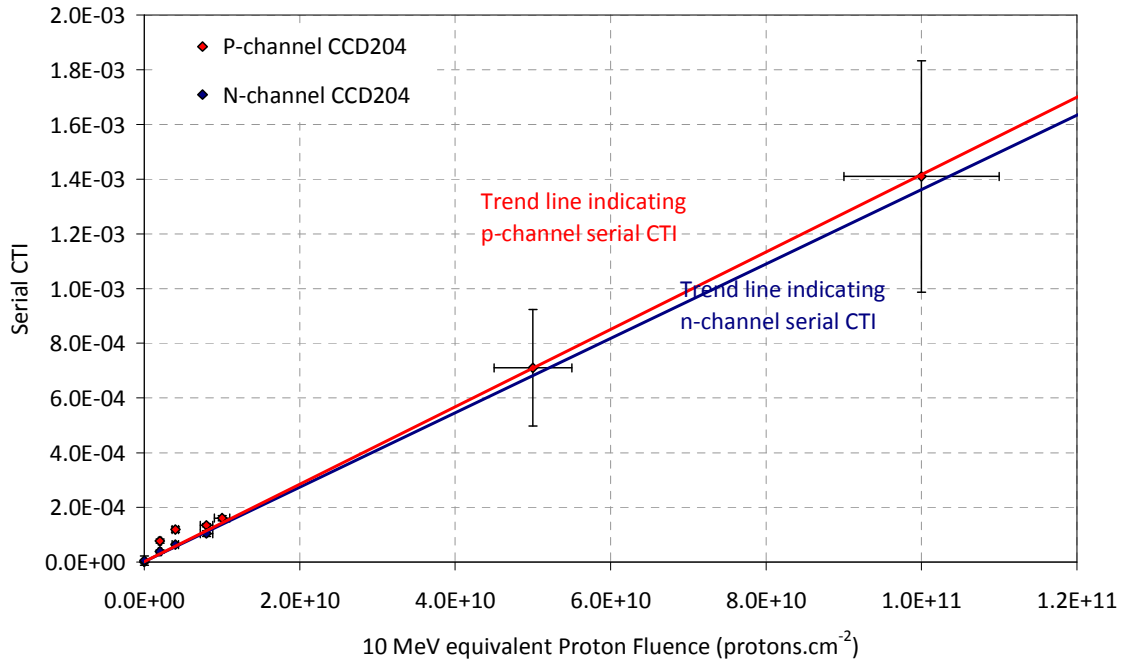
Figure 9.4: Comparison of the serial CTI measuring using the p-channel with an n-channel CCD204 at 150 K
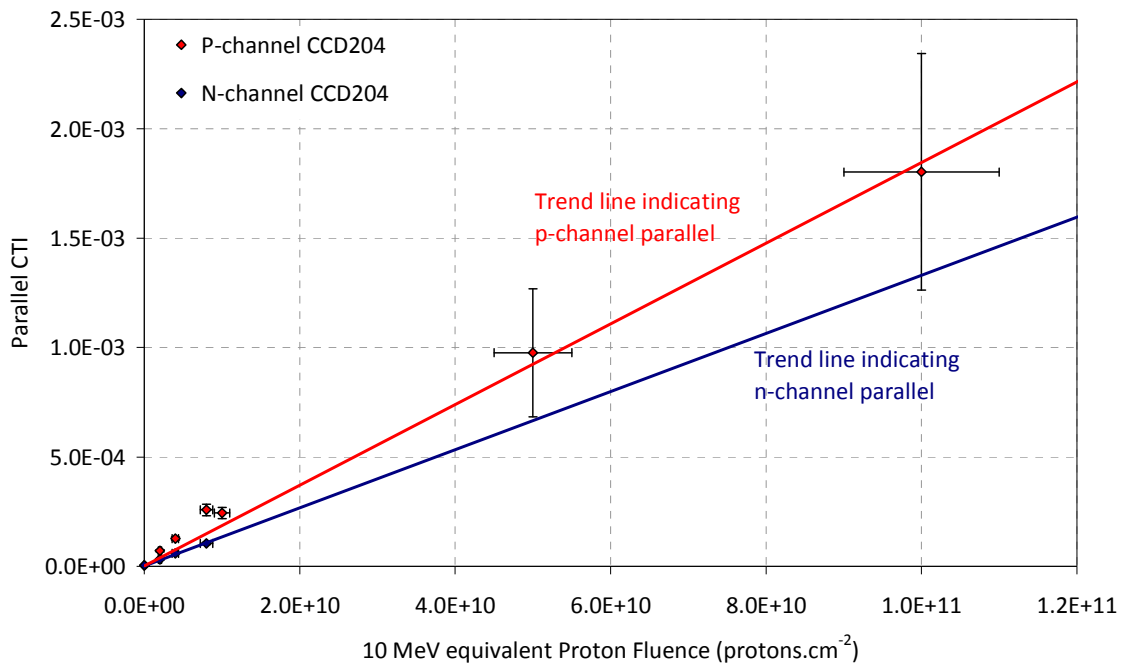
Figure 9.5: Comparison of the parallel CTI measuring using the p-channel with an n-channel CCD204 at 160 K
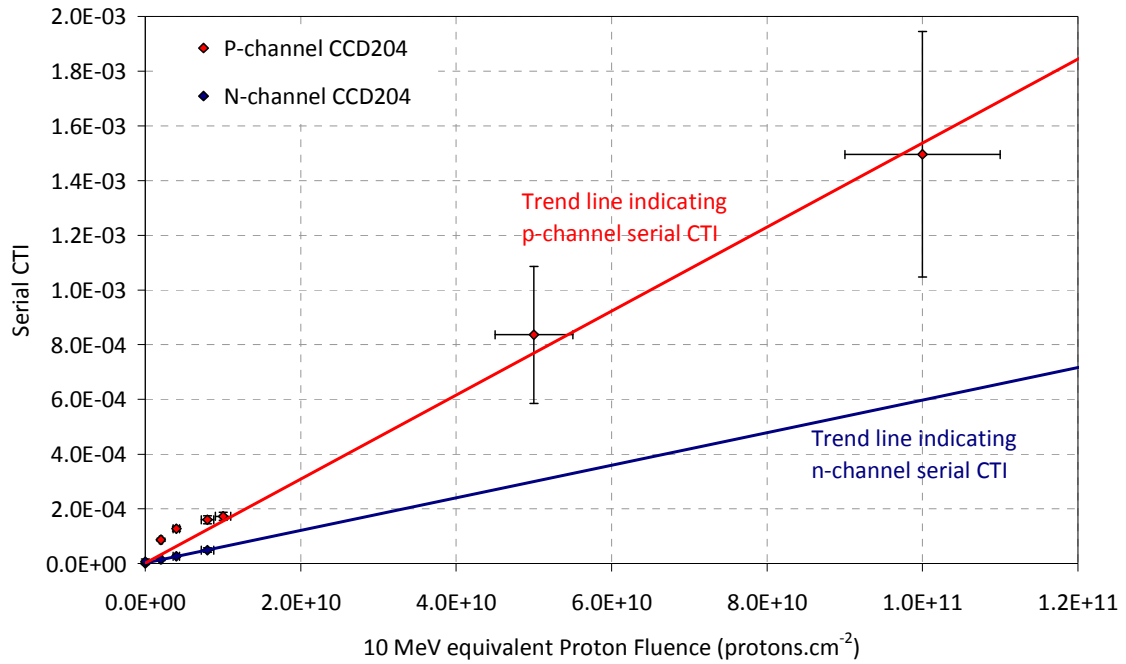
Figure 9.6: Comparison of the serial CTI measuring using the p-channel with an n-channel CCD204 at 160 K

The average radiation damage constant, given by the change in CTI as a function of the proton fluence delivered, for the nominal Euclid operating temperature range is given in Table 4. The difference between n-channel and p-channel RDC is also given, where below 1 the n-channel outperforms the p-channel and above 1 the p-channel outperforms the n-channel. The difference in the parallel and serial RDC as a function of temperature is illustrated in Figure 9.7. It appears that under current operating conditions the p-channel CCD204 provides a reduction in tolerance to radiation induced CTI.

	160 K			150 K			140 K		
	N-channel	P-channel	Change	N-channel	P-channel	Change	N-channel	P-channel	Change
Parallel RDC	1.3E-14	2.6E-14	0.5	1.1E-14	3.1E-14	0.3	9.9E-15	3.3E-14	0.3
Serial RDC	4.8E-15	2.4E-14	0.2	1.5E-14	2.1E-14	0.7	3.2E-14	1.5E-14	2.1

Table 4: Average radiation damage constant measured over the nominal Euclid operating temperature range
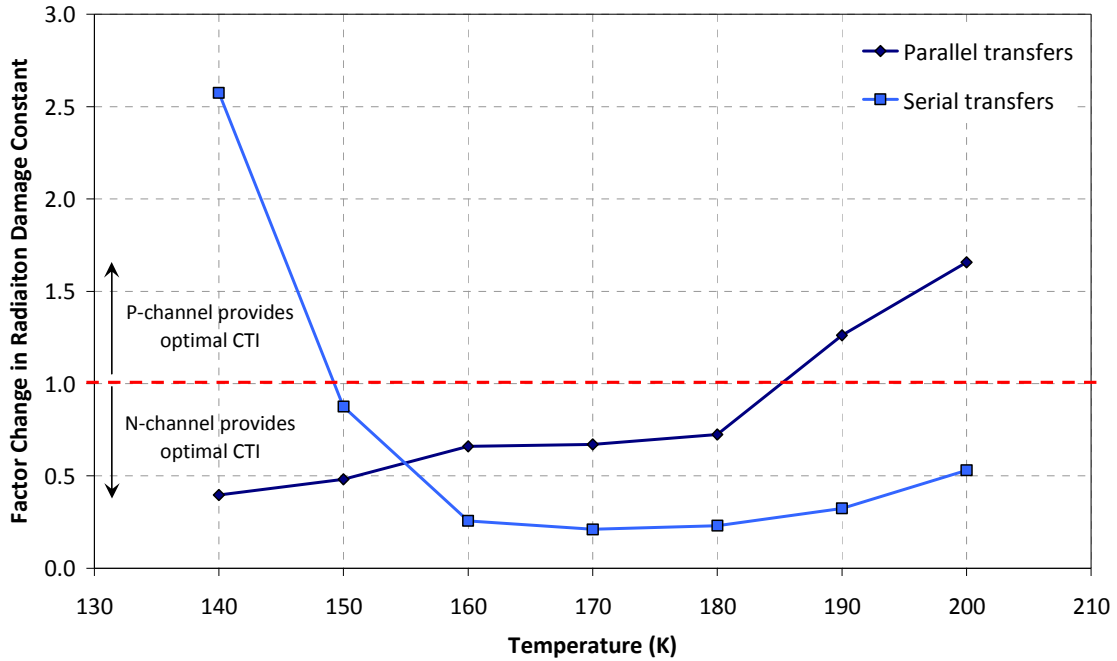
Figure 9.7: Comparison of the difference in parallel and serial RDC values for the n-channel and p-channel CCD204 devices

10 Conclusions

The pre-irradiation performance of the p-channel CCDs is comparable to the n-channel equivalent, demonstrating a clear improvement in this new p-channel CCD technology from e2v.

The performance of this batch of p-channel CCD204s under a direct comparison with n-channel CCD204s post-irradiation from an earlier study initially does not appear to demonstrate the benefits indicated by previous comparative studies [4-6].

However, it should be noted that the operating conditions, i.e. readout rate and clocking scheme, were selected for use from the Euclid project and were optimised for an n-channel CCD. As the CTI in p-channel CCDs is affected by different trap species from those in n-channel, the performance of the p-channel CCD204 will benefit from a detailed investigation into the radiation induced traps in p-type silicon. This will allow the optimal charge transfer timings to be selected, which should be followed by an exploration into more mission specific applications and the development of charge transfer models for use with p-channel CCDs. The next stage in p-channel development should also include the production of further devices using the same mask set as an existing n-channel CCD, e.g. the CCD273, to demonstrate repeatability of manufacture and device performance and to further our understanding of p-channel CCD operation.

Preliminary testing into the clocking optimisation of these p-channel devices has indicated that a further factor of 4× improvement compared to n-channel technology may be within our grasp following a detailed study.

The change in the CTI behaviour of the control regions is noteworthy and is likely to be the result of neutron damage. The increase in CTI and dark current in the control regions is small when compared to the increase in the irradiated regions; therefore the main damage component is the

protons. However, irradiating new devices, using lower energy protons to reduce the neutron flux would be of benefit.

Further work should include:

- Investigate trap species present within the CCD, pre and post irradiation, possibly through the use of pocket pumping and EPER.
- Annealing tests to help verify the trap species identification.
- An investigation into the optimisation of p-channel CCD CTE, for example using different clocking schemes, CDS timings and readout speeds. A detailed study was performed on the n-channel CCD204; however the p-channel CCD204 has not received a comparable level of optimisation at this time.
- Perform a cryogenic irradiation, with the possibility of performing long term monitoring with the CCD cold.
- Development of a charge transfer model for p-channel CCDs, based on trap parameters identified in the further work described above and verified against experimental data generated specifically for model verification.
- Perform evaluations of post-irradiation performance using both X-ray and optical stimulation, to represent test conditions used in future instrumentation and to demonstrate the benefits of the new technology.
- Produce a second p-channel CCD using an existing n-channel mask set, e.g. the CCD273, to ensure device performance is repeatable and to further our understanding of p-channel CCDs.
- Investigate the observed changes to the control regions, possibly using a readily available CCD to examine changes in performance under different irradiation conditions and under direct neutron irradiation.

11 Acknowledgments